PHYSICAL LAYER SECURITY IN THE VISIBLE LIGHT COMMUNICATIONS SYSTEMS

EKİN BAŞAK BEKTAŞ

MASTER'S THESIS

Submitted to the School of Graduate Studies of
Kadir Has University in partial fulfillment of the requirements for the degree of
Master of Science in Electronics Engineering

İSTANBUL, JULY, 2020

DECLARATION OF RESEARCH ETHICS /
METHODS OF DISSEMINATION

I, EKİN BAŞAK BEKTAŞ, hereby declare that;

- this master's thesis is my own original work and that due references have been appropriately provided on all supporting literature and resources;
- this master's thesis contains no material that has been submitted or accepted for a degree or diploma in any other educational institution;
- I have followed *Kadir Has University Academic Ethics Principles prepared in accordance with The Council of Higher Education's Ethical Conduct Principles.*

In addition, I understand that any false claim in respect of this work will result in disciplinary action in accordance with University regulations.

Furthermore, both printed and electronic copies of my work will be kept in Kadir Has Information Center under the following condition as indicated below:
The full content of my thesis will be accessible from everywhere by all means.

EKİN BAŞAK BEKTAŞ
09/07/2020

KADİR HAS UNIVERSITY

SCHOOL OF GRADUATE STUDIES

ACCEPTANCE AND APPROVAL

This work entitled PHYSICAL LAYER SECURITY IN THE VISIBLE LIGHT COMMUNICATIONS SYSTEMS prepared by EKİN BAŞAK BEKTAŞ has been judged to be successful at the defense exam on 09/07/2020 and accepted by our jury as master's thesis.

APPROVED BY:

Prof. Erdal PANAYIRCI (Advisor) .....
Affiliation of the Advisor

Prof. Mutlu KOCA .....
Affiliation of the Examiner

Assoc. Prof. Dr. Serhat ERKÜÇÜK .....
Affiliation of the Examiner

I certify that the above signatures belong to the faculty members named above.

.....

Dean of School of Graduate Studies

DATE OF APPROVAL: 09/07/2020

TABLE OF CONTENTS

PHYSICAL LAYER SECURITY IN THE VISIBLE LIGHT COMMUNICATIONS SYSTEMS

ABSTRACT

With the rapid developments in technology in recent years, the need for fast and secure access to information has been increasing day by day. With this increasing demand, the radio frequency (RF) band which used for wireless communication is rapidly filling and even the limit is approached. Therefore, this increasing need day by day has led to the emergence of a new research area. Many researchers from both academia and industry are looking for an alternative route. Visible light communication (VLC) is a strong candidate to meet this demand due to its advantages such as broad bandwidth visible light spectrum (340 THz to 790 THz), the spectrum's openness for license-free use, the high-speed data transfer and the security it provides. For this reason, issues such as estimation of realistic optical channel used in VLC systems and analysis of their performance have gained importance. Apart from the security that VLC systems provide for single users in closed areas, studies are carried out to ensure security in common areas (eg.; airports, shopping malls, offices etc.) and in multi-user scenarios. Accurate estimation of the channel used is also very important for this security performance analysis. The main purposes of this thesis is to make the physical layer security (PLS) scheme more applicable for situations where the channel is not fully known, as in real life applications, and to increase the security capacity. in addition to those, to present a performance analysis for VLC systems under the presence of different clipping noises of a new channel estimation method for DCO-OFDM systems, a type of optical OFDM.

Keywords: Visible Light Communication (VLC), Physical-Layer Security (PLS), Orthogonal Frequency Division Multiplexing (OFDM), DC-Biased Optical Orthogonal Frequency Division Multiplexing (DCO-OFDM), Clipping Noise, Channel Estimation.

GÖRÜNÜR IŞIKLA HABERLEŞME SİSTEMLERİNDE FİZİKSEL KATMAN GÜVENLİĞİ

ÖZET

Son yıllarda teknolojideki hızlı gelişmelerle birlikte bilgiye hızlı ve güvenli erişime olan ihtiyaç da gün geçtikçe artmaktadır. Artan bu taleple birlikte kablosuz haberleşme için kullanılmakta olan radyo frekans (RF) bandı hızla dolmakta ve hatta sınıra yaklaşılmaktadır. Dolayısıyla günden güne artmakta olan bu ihtiyaç yeni bir araştırma alanının doğmasına sebep olmuştur. Gerek akademi gerekse sanayiden birçok araştırmacı alternatif bir yol aramaktadır. Görünür ışık haberleşmesi, geniş bant genişliğine sahip görünür ışık spektrumu (340 THz to 790 THz), bu spektrumun lisanssız kullanıma açık olması, sağladığı yüksek hızlı veri transferi, ışığın kapalı ortamdan dışarı çıkamama özelliğinin sağladığı güvenlik gibi avantajları nedeniyle bu talebi karşılama açısından güçlü bir aday olarak kabul edilmektedir. Bununla birlikte, VLC sistemlerde kullanılan gerçekçi optik kanalın tahmini ve başarımlarının analizi gibi konular önem kazanmıştır. VLC sistemlerinin kapalı alanlarda tek kullanıcı için sağladığı güvenlik dışında ortak alanlar (ör; havaalanları, alışveriş merkezleri, ofisler vb.) ve çoklu kullanıcılı senaryolarda güvenliği sağlamak adına çalışmalar yapılmaktadır. Kullanılan kanalın doğru tahmini bu güvenlik performansı analizi için de oldukça önemlidir. Bu tezin temel amacı, fiziksel katman güvenlik (PLS) şemasını gerçek hayat uygulamalarında da olduğu gibi kanalın tamamen bilinmediği durumlar için daha uygulanabilir hale getirmek ve güvenlik kapasitesinin artırılmasının yanı sıra optik OFDM'in bir türü olan DCO-OFDM sistemleri için yeni bir kanal tahmin yönteminin farklı kırpma gürültülerinin varlığı altındaki VLC sistemleri için bir performans analizinin sunulmasıdır.

Anahtar Sözcükler: Görünür Işıkla Haberleşme(VLC), Fiziksel Katman Güvenliği (PLS), Dikey Frekans Bölmeli Çoğullama (OFDM), DC-öngerilimli optik OFDM (DCO-OFDM), Kırpma Gürültüsü, Kanal Kestirimi.

ACKNOWLEDGEMENTS

I would like to express my sincere gratitude to my thesis supervisor, Prof. Erdal Panayirci who has supported me throughout my graduate studies not only for preparation of this thesis but also for every decision I have made. Without his guidance and knowledge I would not be able to complete my master's study. His endless energy and motivation be a lesson to us all.

I would like to thank Prof. Harald Haas who is known as "Father of Li-Fi" to hosted me for 2 months in his Li-Fi R&D Lab at The University of Edinburgh. It was an invaluable experience for me. I am very grateful to get a chance to work with him. I also thank the other researchers at my faculty and thank my friend for their understanding.

I gratefully acknowledge the Kadir Has University, Department of Electrical - Electronics Engineering funding and Prof. Dr. Erdal Panayirci's research grant from the TUBITAK 1003 Priority Areas R&D Project, "Physical Layer Security in Visible Light Communication System", Project No: 218E034 for providing me financial support throughout my graduate studies. I have served as a teaching assistant in the Department of Electrical - Electronics Engineering at Kadir Has University and a research assistant in Prof. Panayirci's project during my master degree.

Last but not the least; I would like to express my thankfulness to my parents, my sister and my brother-in-law. The unconditional support of them gave me the strength to carry out my thesis and to finish it. Especially on these coronavirus days I could not finish my graduate studies without psychological support they provide.

To my parents

LIST OF TABLES

LIST OF FIGURES

LIST OF SYMBOLS/ABBREVIATIONS

B	Clipping Noise
$\lceil . \rceil$	Ceiling Operator
$\lfloor . \rfloor$	Floor Opeartor
N_{cp}	Length of Cyclic Prefix
OWC	Optical Wireless Communication
VLC	Visible Light Communication
IoT	Internet of Things
5G	5th Generation
LED	Light Emmiting Diode
LASER	Light Amplification by Stimulated Emission of Radiation
OFDM	Orthogonal Frequency Division Multiplexing
OFDM-IM	Orthogonal Frequency Division Multiplexing Index Modulation
OSM	Optical Spacial Modulation
OSSK	Optical Space Shift Keying
CSI	Channel State Information
PLS	Physical Layer Security
NOMA	Non-Orthogonal Multiple Access
DCO-OFDM	Direct Current Biased Optical Orthogonal Frequency Division Multiplexing
Li-Fi	Light Fidelity
RF	Radio Frequency
OGSSK	Optical Generalized Space Shift Keying
SISO	Single-Input Single-Output
MIMO	Multiple-Input Multiple-Output
SM	Spatial Modulation
PD	Photodiode
AWGN	Additive White Gaussian Noise
ML	Maximum Likelihood

M-QAM	M-level Quadrature Amplitude Modulation
M-PSK	M-level Phase Shift Keying
FFT	Fast Fourier Transform
IFFT	Inverse Fast Fourier Transform
CP	Cyclic Prefix
MSE	Mean Squared Error
BER	Bit Error Rate
SER	Symbol Error Rate

1. INTRODUCTION

1.1 History of the Visible Light Communications

Optical wireless communication (OWC) is a one of the oldest technologies still in use today. The reflection of sunlight and fire signs was used by the Romans, and Greeks as signal in 800 BC and smoke patterns were used by Americans for long-distance communications in 150 BC. The invention of the optical telegraph by the French inventor Cloude Choppe in 1792, likewise, in 1880, Graham Bell invented the photo-phone to transmit voice by using the sunlight and selenium cell in the receiver to demodulate audio signals, and vibrating mirrors to module the voice signals [1]. These inventions are extremely important in terms of optical wireless communication.Despite these developments, Light Amplification by Stimulated Emission of Radiation (LASER) was caused to the popularization of the OWC. Visible light communication (VLC) is an optical communication type that uses the visible light spectrum in the frequency range from 340 THz to 790 THz. VLC has emerged as a promising wireless technology that combines data communication and illumination. In VLC, the information is transmitted by modulating the intensity of the light emitting diodes (LEDs) at high frequencies, making instant changes in the intensity of light that cannot be detected by the human eye. In 2003 at the Nakagawa Laboratory which located in Keio University in Japan, data transmission was carried out using LEDs [2]. In recent years, VLC has gained significant interest because of the high speed, license-free frequency spectrum, lower power consumption and higher efficiency it provides [3, 4].

Date	Systems, Devices, Standards
800 BC	Fire Beacons by the Greeks and Romans
150 BC	Smoke Signal by the Amerikans
1792	Optical telegraph by the French inventor Cloude Choppe
1880	Photophone by A. Graham Bell
1960	LASER by Theodore H. Maiman
1970s	FSO (Free-Space Optics) used in secure military applications
1979	Indoor OWM systems by F. R. Gfeller and G. Bapst
1993	Open standard for IR data communications (IrDA)
2003	The Visible Light Communication Consortium
2008	OMEGA Project
2009	IEEE802.15.7 Standard on VLC

Table 1.1 Optical Wireless Communication Timeline

1.2 Physical-Layer Security

In recent years, issues such as the security and priority of information have become a very important issue as there is much more information traffic on wireless networks than expected. In indoor optical wireless communication as light cannot not pass through walls, it is not possible for the information signal to leak outside of the room. However, it is still possible for eavesdroppers to listen to the communication links in the shared areas or through surfaces that allow light to pass, such as glass windows [5]. Secrecy capacity can be defined simply as the maximum speed of reliable source-to-target confidential data transmission, while information is completely hidden from eavesdroppers. In literature, there has been many studies that focus on physical layer security for Gaussian wiretap channels, in [6], Wyner characterized the secrecy capacity for single-input single-output Gaussian wiretap channels, in [7] secrecy capacity was achieved for the Gaussian wiretap channel by Leung-Yan-Cheong and Hellman. In VLC channels, transmitted signals must be real and positive valued because of the limited dynamic range of the LEDs, the system is imposed by an amplitude constraint on the channel input which makes it difficult

to obtain closed form expressions for the secrecy capacity [8].

1.3 Motivation

With the developing technology, the need for fast and reliable access to information is increasing day by day. These two requirements have become more of an issue, especially with Internet of Things (IoT) and 5th Generation (5G) Communication. The lack of capacity to meet demand with such a significant increase in Radio Frequency (RF) technology used today has pushed researchers to look for new technologies with this capacity. As a candidate for this, VLC is one of the technologies that can be used for data communication in terms of high data rate, high connection density and security. VLC is more reliable than other communication systems because of the light cannot pass through the wall. Nevertheless, this feature of light is not sufficient to ensure safety considering shared areas (e.g. offices, shopping malls, libraries etc.) or communication scenarios with many users. In light of this idea, the studies in this thesis aim to increase the physical layer security in VLC, both theoretically and practically, taking into consideration the realistic channels between OWC connections.

1.4 Contribution of the Thesis

Thesis contributions can be listed as follows:

1. By taking into account the uncertainty on the channel, we design some new technique for physical-layer security whose performance is more feasible in real life scenarios where channel information is never fully known.
2. An efficient and fast iterative method is proposed to estimate the channel for DCO-OFDM based VLC system in presence of clipping noise. Bit error rate(BER) versus signal-to-noise ratio (SNR) performances are analyzed and compared their performances with the perfect CSI case as well as with the estimated channel which is obtained from the proposed method. This work

published in [9].

3. It has been proposed a new physical layer security technique with Optical Generalized Space Shift Keying (OGSSK) based VLC systems and the performance of the algorithm is investigated by computer simulations. It yielded a very good error performance in the presence of perfect CSI situation, under possible noises in the channel.
4. The proposed algorithm was also tested in the presence of imperfect CSI and it was concluded that the algorithm performs well in providing physical security for the legitimate user.

1.5 Thesis Outline

In **Chapter 1**, literature review for VLC and PLS for OWC is presented and the thesis's motivation is given. In **Chapter 2**, working principle of VLC is introduced, including IM/DD structure, Light Emitted Diode (LED) and Photodiode (PD) which are used as transmitter and receiver, respectively. In **Chapter 3**, used physical layer security techniques in VLC systems are given in detailed. In **Chapter 4**, our recent research results on PLS with OGSSK based VLC systems are presented. In **Chapter 5**, a new channel estimation algorithm is proposed and simulation results are given. In **Chapter 6**, PLS algorithm performances in the presence of the channel estimation errors are shown.

2. PRINCIPLES OF VISIBLE LIGHT COMMUNICATION

Optical wireless communication is a general name given in technology where light is used to provide for transmission of information in wireless communication. On the other hand, free-space optics (FSO) is used in OWC to provide long-range communication, infrared rays (IR) are used in short range communication. In VLC, the visible light acts as an optical carrier for information transfer. While LEDs are used as transmitter in VLC, PDs are used as receiver that have very good responsiveness in visible light wavelength. In VLC, for both indoor and outdoor communication, air is used as communication medium and also the signal transmitted in VLC has a positive and real characteristic. The basic block diagram of a VLC structure is shown in Figure 2.1. As it is seen from Figure 2.1, the system consists of a transmitter, channel and a receiver modules with white Gaussian noise that always exists in the system.

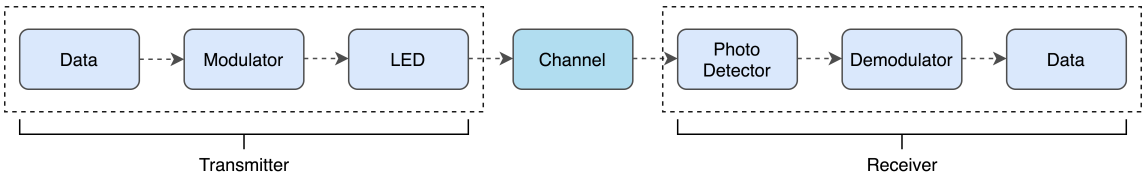

Figure 2.1 Basic Block Diagram of the VLC System

In a VLC system, the received signal can be expressed as

$$\mathbf{r(t)} = \mathbf{Hs(t)} + w(t) \tag{2.1}$$

where H represents the channel, $s(t)$ represents the transmitted signal that carries data, and $w(t)$ denotes additive white Gaussian noise (AWGN). As shown in Figure 2.2, a VLC system model has three domains of which the two of them are electrical the other one is optical. As seen in the figure, the transmitter generates a modulated signal, added to a direct current (DC) providing the necessary power to drive the

LEDs. While the LED in the environment provides illumination, it also transmits data. In the air, which is used as communication medium, light rays follow some line-of-sight(LOS) paths. The phase detector (PD), which forms part of the receiver, receives the signal to which a Gaussian noise is also added and converts it into an electrical signal. The information is transmitted to the user after demodulating at the receiver.

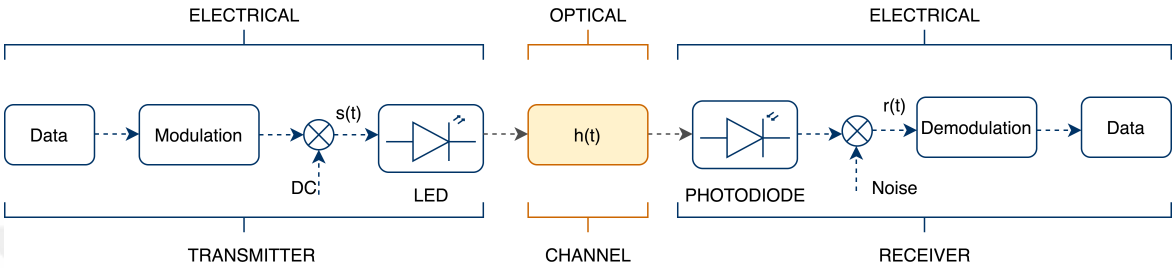

Figure 2.2 VLC System Model

2.1 Transmitter of a VLC System

LEDs are used as means to transmit optical signals in VLC systems. Advances in LED technology have made optical communication advantageous over other candidates. The LEDs serve to convert the modulated electrical signal in the transmitter into an optical intensity value. Two types of LEDs are used in VLC, one is a single-color LED and the other is a multi-color Red-Green-Blue (RGB) LED. Each antenna is represented by a LED color. The number of channels in a VLC system and the number of LEDs are related with each other. Therefore, the number of channels in the system will be equal to the number of colored LEDs. RGB LEDs are used as multi-channel transmitters to apply multi-carrier modulation techniques. In Figure 2.3, transmitter part of a VLC system is shown.

2.2 VLC Channel

Infrared links configurations have six different types [10]. The obstacles in the path of light, and direction of the transmitter and receiver cause different types of links in the transmission medium. Namely, directed Line-of-Sight (LOS), non-

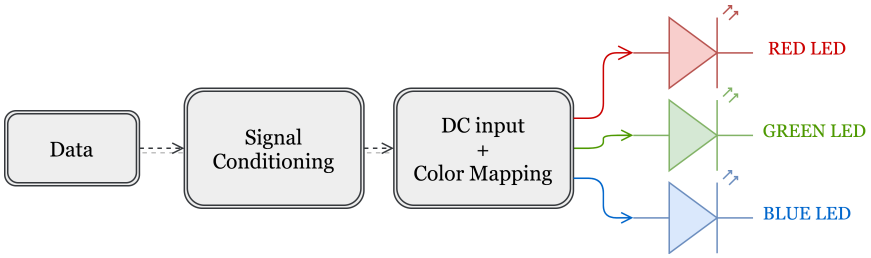

Figure 2.3 Transmitter Part of a VLC System

directed LOS, directed Non-Line-of-Sight (N-LOS) and non-directed (NLOS) are the main link types. Hybrid links are also exist. According to the direction of the transmitter and receiver, directed or non-directed links are occur. Whether the link is NLOS or LOS depends on the obstacles between the transmitter and receiver. An indoor VLC scenario shown in Figure 2.4. The link between the transmitter and the receiver is assumed to be a LOS link.

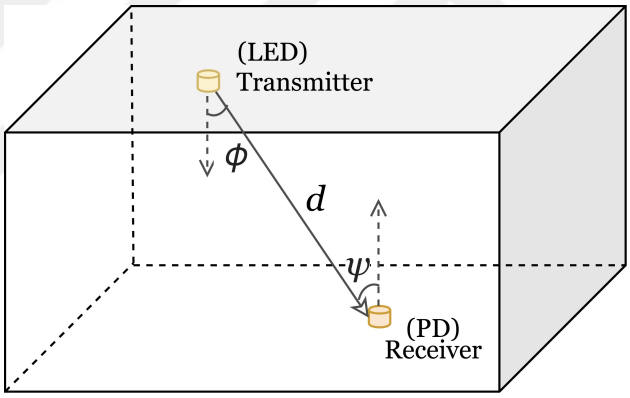

Figure 2.4 Geometry of an indoor VLC scenario with non-directed LOS link

The LOS channel impulse response $H(0)$ is expressed as [10, 11];

$$H(0) = \frac{(m+1)A}{2\pi d^2} \cos^m(\phi) T_s(\psi) g(\psi) \cos(\psi), \qquad 0 \leq \psi \leq \psi_c \tag{2.2}$$

In this equation, m denotes the Lambertian emission order; A represents the physical area of the PD. The distance of LOS link between receiver and transmitter is represented by d. $T_s(\psi)$ and $g(\psi)$ are represent optical filter gain and non-imaging concentrator, respectively. The transmitter's location is determined by the angle of irradiance ϕ. Angle of incidence to the receiver surface relative to the normal axis

is ψ. ψ_c indicates the width of the field of view (FOV) of the PD.

Lambertian order emission m, the LED's semiangle the half-power can be expressed as follows [10, 11];

$$m = \frac{\text{-ln2}}{\ln \cos \phi_{1/2}} \tag{2.3}$$

2.3 Receiver of a VLC System

The message that comes out as an electrical signal from the user, is converted to an optical signal at the output of the LED driving circuit and passes through the optical channel and reaches the receiver block of the VLC system. After such processing as demodulation, decoding and detection in the receiver, detected data is delivered to the user. As a photodetector (PD) device in VLC systems, photodiode and image sensors can be used. However, photodiode is widely adopted in real applications since it is more cost effective. As shown in Figure 2.5, the receiver part of VLC systems consists of concentrator, optical filter, photodetector, amplifier, equalizer and electrical filter. The purpose of using a concentrator here is to allow more light to enter the receiver block. Light rays pass through the concentrator and optical filter before reaching the photodetector. The signal reaching the PD passes through the amplifier and equalizer. After these processes, the signal, in which noise is added, reaches the user in the form of light current.
The power of the signal obtained in the receiver can be expressed as;

$$P_r = H(0).P_t \tag{2.4}$$

where P_t represents the transmitted power and $H(0)$ is the LOS channel impulse response as defined in equation 2.2.

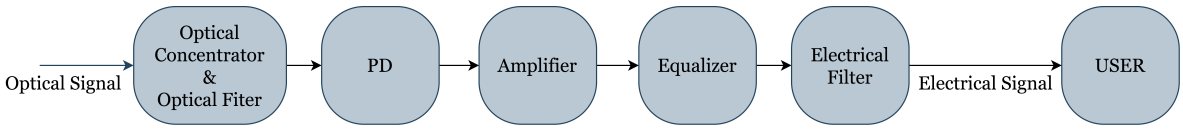

Figure 2.5 Receiver Part of a VLC System

2.4 VLC vs. IR Communication

	VLC	**IR Communication**
Status	IEEE 802.15.7	IrDA Standardization
Data Rate	>100Mb/s possible	4Mb/s(FIR),16Mb/s(VFIR)
Carrier-Wavelength	375 nm-780 nm	850 nm-900 nm
Security	Good	Good
Distance	Short-Range (∼meters)	Short-Range (∼3 meters)
Service(s)	Illumination, Communication	Communication
Noise Source(s)	Sun Light, Other Light Sources	Ambient Light
Applications	Indoor Communication, V2V Communication	Remote Control, Point-to-Point Connection

Table 2.1 Comparison of VLC and IR Communication

On the other hand, IrDA (Infrared Data Association) standardized infrared (IR) communication. Infrared communication's data rate is 4 Mb/s for fast infrared (FIR) and 16 Mb/s for very fast infrared (VFIR) [12, 13]. In VLC, data rate is rely on the modulation bandwidth of LEDs and it can be defined as >100 Mb/s. Although both technologies provide short-range communication, it can be said that VLC provides communications up to several meters due to the lighting requirement. On the other hand, maximum distance that infrared rays can be employed is 3 meters. The light emission of VLC system data with a separate wavelength for each color from red to violet makes the VLC systems more complex than infrared communication. In IR communications, ambient light causes noise. However, in VLC, sunlight and other light sources can cause a Gaussian type of noise. VLC is expected to be used in indoor communications and in vehicle-to-vehicle (V2V) communications in the near future.

3. PHYSICAL LAYER SECURITY IN VISIBLE LIGHT COMMUNICATION

In recent years, with the developments in the communications technology, the technologies such as IoT and device-to-device (D2D) communications have begun to enter our lives, and demand for fast and secure access to information has been increasing day by day. Thus, in addition to researches aimed at increasing the data rate in wireless communications, studies on the data security and privacy of these systems have also gained vital importance. In particular, communication in multi-user scenarios as well as in common areas (e.g. airports, aircraft, hospitals, offices etc.) including unauthorized users have been widespread realized. Disorders such as fading and noise in wireless channels can be employed to implement security in PLS systems. In the Seminal paper which is published in 1949 [6], Shannon laid the foundations of cryptography secrecy. The first studies on physical layer security in the field of information theory started with Wyner introducing a channel model which he called "Wire-Tap" for this purpose [7]. A wire-tap channel model is shown in Figure 3.1. In this channel model, it is assumed that a degraded version of the signal transmitted from the transmitter reaches the unauthorized user. The distorted listening channel model was later expanded by Csiszár and Körner, and a new broadcast channel model was developed in which communication was carried out intact [14]. In the studies, carried out in this context, showed that under the assumption that the signal transmitted to the authorized user is less disturbed, perfect confidentiality can be ensured and the privacy capacity of the system can be calculated by taking the difference of the information capacity of authorized and unauthorized users.

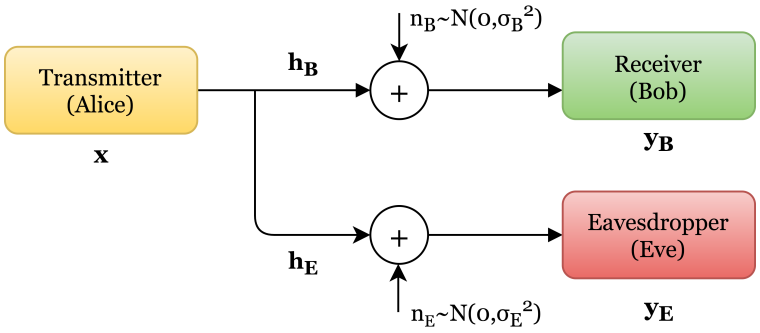

Figure 3.1 Wire-Tap Channel Model

3.1 PLS in VLC

Physical layer security is a security scheme that uses the differences between the user's channels to hide data from eavesdropper while transmitting information to the authorized user, without relying on the encryption methods in the upper six layers, when the OSI layers are considered. Unlike conventional RF communication, which operates under the influence of power constraint and Gaussian noise, VLC transmits information to the receiver through optical signals generated by the light intensity emitted by the LEDs. In the receiver side, exact information is extracted from these signals with the help of photo-detectors. Optical signals transmitted in VLC are real and positive, as they are modulated by the intensity of the emitted light. In addition, the fact that the LEDs used for this purpose have limited operating characteristics in the linear region and must provide sufficient illumination of the environment, imposes the restriction of the average or peak amplitudes of the transmitted optical signals [15, 16, 17]. In general, although typical LEDs have nonlinear electrical-optical transfer properties, this linearity problem has been shown in [18] to be easily solved by a suitable pre-distortion technique. In communication systems, secrecy capacity can be described as the maximum amount of information that can be transmitted between the reliable source-to-target while confidential information is totally hidden from eavesdropper. Since the visible light wavelength is very short compared to the sensing surface of a typical photo-detector on the receiving side, the multi-path fading effect resulting from the propagation of RF waves does not occur in the VLC and is generally assumed that the communication between the

receiver and transmitter is provided by LOS link. Due to these fundamental differences between RF and VLC, the secrecy capacity results obtained for RF networks cannot be applied directly to VLC networks. Since the confidentiality capacity of a VLC system is related to the channel capacity of the communication channel in that system, first of all, mean, peak and true-value of the optical channel capacity should be accurately calculated under the positive amplitude constraints [7, 14]. However, in VLC systems, even for single-input-single-output (SISO) channels, exact formulation that can precisely calculate channel capacity under these constraints has not been developed. In [19], Shannon mentioned the difficulty of analytic expression of unlimited channel capacity for Gaussian wiretap channels with amplitude constraints, instead he obtained a lower bound and an asymptotic upper bound for high SNR. Instead, studies were carried out in [20, 21, 22, 23, 24] to ensure physical safety and to obtain upper and lower limits. In [20], some numerical results are shown for SISO and MISO cases.

On the other hand, in a typical lighting application, desired lighting level is achieved by using arrays of LEDs. It is shown in [25] that the LiFi networks are 20 times more secure than the WiFi networks in terms of security capacity. To show clearly why this difference is occurred, in Figure 3.2, an example of the two houses are given where one of it is equipped with WiFi and the other one equipped with LiFi. In

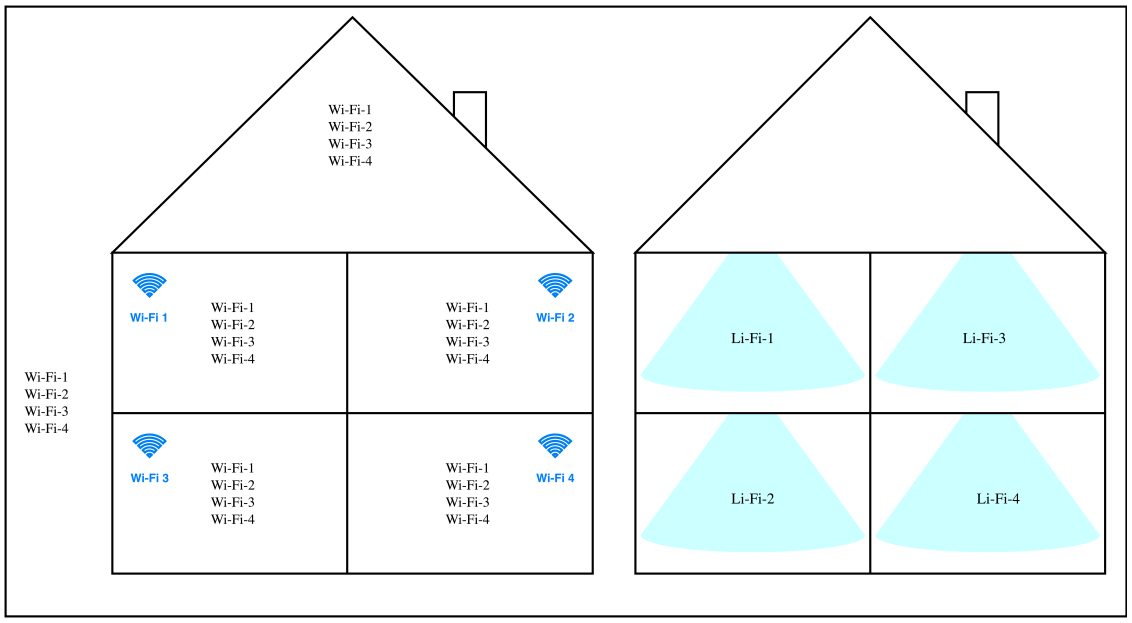

Figure 3.2 Wi-Fi vs. Li-Fi

the house which is equipped with WiFi, signals can be seen from all of three rooms even outside of the house. However, for the other house, because of the light kept in the indoor environment, LiFi signals can not be seen from any other room.

3.1.1 The main techniques for PLS

Some physical layer security techniques can be devised. Such as,

Generating Jamming Signals:. In order to secure the message sent from the transmitter, a distorting signal is also sent in addition to the sent message. This signal is called "jamming" signal. While the jamming signal makes the signal received by the eavesdropper meaningless, no distortion occurs in the signal received by the user, as it is transmitted to the legal receiver's null-space. Thus, physical security is provided.

Applying Beamforming:. In this approach, the transmitted signal power is divided into two, and a narrow optical beam is created with an LED array on the transmitter in line with the authorized user and the information signal is transmitted in such a beam [26]. Here, although there is no need to know the channel information of the eavesdropper, there will be large losses in the power efficiency of the system, since this time some of the power of the signal transmitted from the source to the user is used for beamforming purpose.

Applying Some Modulation Techniques:. Recently, it has been found that some new emerging signal modulation techniques have been quite effective in PLS systems. It is known that these modulation schemes are based on an operation scheme in which information is carried by the labels or indexes of the antenna or LED elements. Consequently, these elements must be switched from one antenna (LED) to the other one in every signaling interval during transmission of data. It has been observed that this random switching operation generates a friendly jamming

signal that cannot effect the legitimate user but severely distorts the confidential information received by the eavesdropper [27], [28]. Those techniques called Index Modulation (IM) are the followings:

- *OFDM Index Modulation (OFDM-IM)* : the indices of the subcarriers of an OFDM system and the symbols transmitted from these subcarriers carry information.
- *Optical Spacial Modulation (OSM)* : the indices of the transmit antennas of a MIMO system and the data symbols transmitted from these antennas carry information.
- *Optical Space Shift Keying (OSSK)* : a special form of SM and the indices of the transmit antennas of a MIMO system carry information only.

3.2 PLS Techniques in VLC Scenarios

Different physical layer security techniques in VLC can be studied under different cases. Such as,

- **1)** Physical layer security with one legitimate user and one eavesdropper.
- **2)** Multiuser in large-scale wireless networks in VLC where multiple legitimate users communicating in the presence of multiple eavesdroppers scattered randomly in the indoor facility.

As mentioned previously, there are some basic PLS techniques that are used to provide physical layer security in VLC. These cases and used techniques can be listed as below:

- ***Case 1*** : Channel State Information (CSI) of the eavesdropper (Eve) is known at the transmitter (Alice).
  In this case, it is assumed that transmitter (Alice) has multiple LEDs and CSI of the eavesdropper (Eve) is known at the transmitter side.

Used Technique:

- ***Beamforming*** is used to transmit most of the message energy in the legitimate user direction, thereby increasing the available secerecy capacity.

- ***Case 2*** : CSI of the eavesdropper (Eve) is not known at the transmitter (Alice).

  In this case, it is assumed that transmitter (Alice) has multiple LEDs and CSI of the eavesdropper (Eve) is not known at the transmitter side.

  Used Techniques:

  - ***Jamming Signals***: In such cases, a jamming signal is generated to secure the information. While this signal makes the signal to the eavesdropper meaningless, since these jamming signals are transmitted in the free space of legal users, it affects the signal of the legitimate receiver as little as possible.
  - ***New Modulation Techniques***: As mentioned previously, it has been recent found that Index Modulation techniques can be effectively used for PLS. These modulation techniques given in detail above are I) OFDM Index Modulation (OFDM-IM) [29], II) Optical Spacial Modulation (OSM) [30], III) Optical Space Shift Keying (OSSK) [31] and Generalized OSSSK (GSSK) [32].

3.2.1 Physical Layer Security with One Legitimate User and One Eavesdropper

In this section, when there is only one legitimate user and an eavesdropper, the basic approach will be presented to ensure physical layer security in the VLC. An indoor communication scenario consisting of a transmitter, a legal receiver and an eavesdropper is shown in Figure 3.3. The scenario can be described by the wiretap channel model as shown in the Figure 3.1. Accordingly the received signals by Bob and Eve can be expressed as follows ;

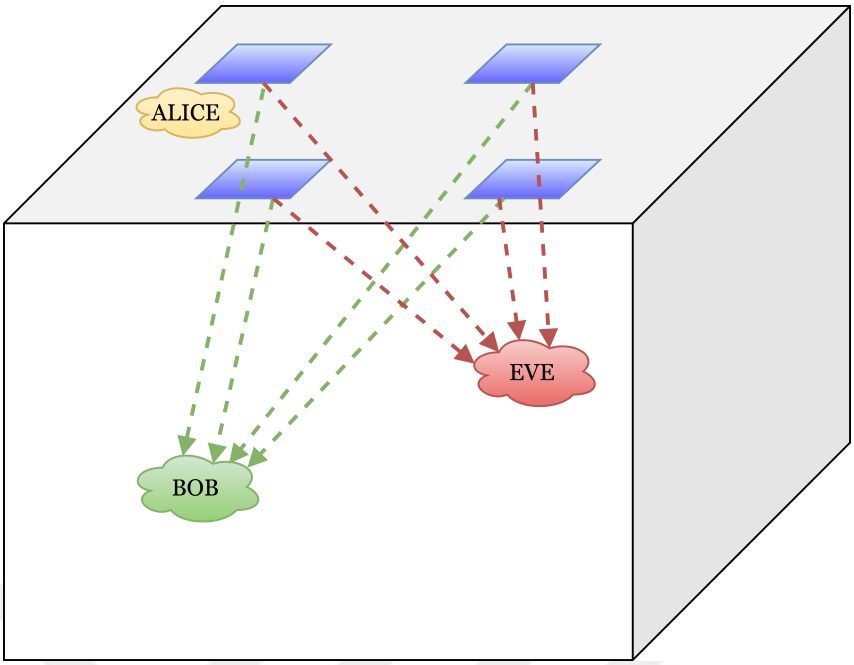

Figure 3.3 An indoor VLC Scenario with One Legitimate User and One Eavesdropper

$$y_B = h_B X + n_B \tag{3.1}$$

$$y_E = h_E X + n_E \tag{3.2}$$

In PLS the other important parameter is the secrecy capacity of the system that can be expressed as,

$$C_s = \mathrm{I}_B(X; y_B) - \mathrm{I}_E(X; y_E), \tag{3.3}$$

where

$$\mathrm{I}_B(X; y_B) = \mathrm{H}_B(X) - \mathrm{H}_B(X|y_B) \tag{3.4}$$

$$\mathrm{I}_E(X; y_E) = \mathrm{H}_E(X) - \mathrm{H}_E(X|y_E). \tag{3.5}$$

Here, $\mathrm{I}_B(X; y_B)$ and $\mathrm{I}_E(X; y_E)$ denote the mutual information per bit. They are related with the entropy of the input symbols for receiver (Bob) and eavesdropper (Eve), $H_B(X)$ and $H_E(X)$ respectively, as well as with the conditional entropies

$H_E(X|y_E)$ between source and receiver .
Hence,

$$C_s = H_B(X) - H_B(X|y_B) - H_E(X) - H_E(X|y_E) \tag{3.6}$$

In this equation, it is clearly seen that to ensure high secrecy capacity we need to reduce the amount of information captured by the eavesdropper.

3.2.2 Multiuser in Large-Scale Wireless Networks in VLC

In this section, PLS techniques for multi-user scenario in large-scale wireless networks in VLC, where multiple legitimate users communicating in the presence of multiple eavesdroppers scattered randomly in the indoor facility, will be presented. As shown in Figure 3.4, a scenario with two legitimate users and an eavesdropper is assumed. In particular, it is considered to apply beamforming to VLC-NOMA (non-orthogonal multiple access) systems for PLS, where it is assumed that a series of reliable cooperative half-duplex relay fixtures have been installed to help secure the transmitted data. The transmitters are equipped with a single light fixtures, containing multiple light emitting diodes, and each receiver is equipped with a single photodetector. To maintain operation within the dynamic range of light emitting diodes, the transmission is amplitude constrained. To superimpose the source's data signal $x \in \mathcal{R}$ on top of a fixed positive bias current that drives its LEDs, intensity modulation is used. Superposition coding is used to transmit two messages to legitimate users. Here x_1 and x_2 represent transmitted messages.

$$x = \alpha|x_1| + (1-\alpha)|x_2|, 0 \leq \alpha \leq 1 \tag{3.7}$$

The weak user first decodes the message caused by the other user as noise; strong user decodes its message through successive interference cancellation (NOMA architecture). Amplitude constraint applied to keep operating in the dynamic range of LEDs:

$$\alpha|x_1| + (1-\alpha)|x_2| \leq A \tag{3.8}$$

As shown in Figure 3.5, the signal received by the weak user (y_W), strong user (y_S)

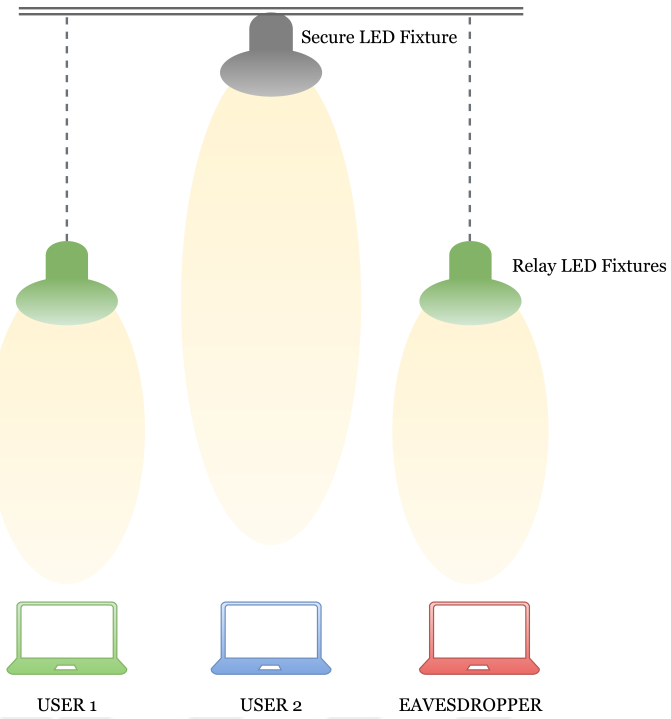

Figure 3.4 Multi-user scenario

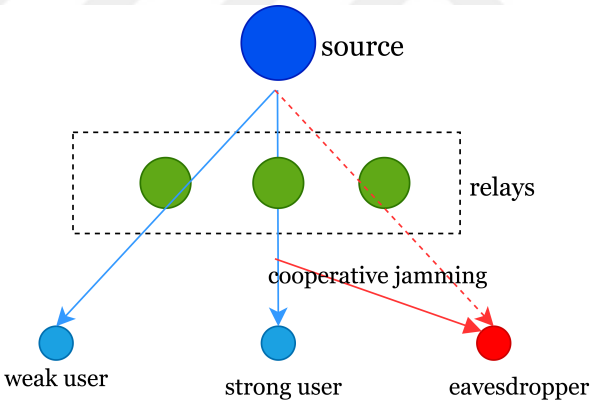

Figure 3.5 An indoor VLC system model: a source fixture communicates with two legitimate users in the presence of an eavesdropper.

and the eavesdropper (y_E) can be expressed as follow;

$$y_W = h_W x + n_W \tag{3.9}$$

$$y_S = h_S x + n_S \tag{3.10}$$

$$y_E = h_E x + n_E \tag{3.11}$$

where h_W, h_S and h_E denote the channel coefficients between the source and the weak user, strong user and eavesdropper, respectively. Similarly, n_W, n_S and n_E represent

the corresponding Gaussian noise signals entering the weak, strong user's channel as well as the noise effecting the eavesdropper. In Figure 3.5, the scheme is shown in which the relays cooperatively transmit a jamming signal, Jz, simultaneously with the transmission of the source. Here, J $\in \mathcal{R}^K$ is a beamforming vector and z is a random variable.

$$|z| \leq \bar{A}$$
$$|\mathbf{J}| \preceq \mathbf{1}_K$$

The random variable z, which represents the common signal of the relays, is uniformly selected in the range of $[\bar{A}, A]$. The beamforming vector should be selected in the free space of the legal users to prevent the generated jamming signal from harming legal users. So,

$$\mathbf{g}_1^T \mathbf{J}_0 = \mathbf{g}_2^T \mathbf{J}_0 = 0$$

by a cooperative jamming for a given alpha, the following secrecy rates can be achievable [25],

$$r_{1,s}^J = \left[\frac{1}{2}\log\left(1 + \frac{2h_1^2\alpha^2A^2}{\pi_e} \right) - \frac{1}{2}\log\left(\frac{1+\frac{h_e^2\alpha^2A^2}{3}+\frac{\left(g_e^T J_0\right)^2\bar{A}^2}{3}}{1+\frac{2\left(g_e^T J_0\right)^2\bar{A}^2}{\pi_e}} \right) \right]^+$$

$$r_{2,s}^J = \left[\frac{1}{2}\log\left(1 + \frac{2h_2^2A^2}{1+\frac{h_2^2\alpha^2A^2}{3}} \right) - \frac{1}{2}\log\left(\frac{1+\frac{h_e^2A^2}{3}+\frac{(g_e^T J_0)^2\bar{A}^2}{3}}{1+\frac{2h_e^2\alpha^2A^2}{\pi_e}+\frac{2(g_e^T J_0)^2A^2}{\pi_e}} \right) \right]^+$$

3.3 Beyond Physical Layer Security

In case of many devices are very close to each other and need to be securely connected to a network at very high speeds, size and magnitude in data density are very important. When compared to radio-based systems like WiFi, it can be said that LiFi is more secure than WiFi. In VLC, **localization** information can be obtained more than RF communication. It is possible to use localization information of light to increase security beyond the physical layer security. In VLC systems, location information of mobile devices or users can be obtained very precisely. Hence, it is possible to record the location information of these devices or people continuously and then statistics obtained with this information can be used to determine the normal motion model of the user. After that, some suitable **machine learning** techniques can be developed to identify any abnormality [25]. On the other hand, the need for connection securely in many workplaces can be utmost necessary. While some business areas can work with more flexible security, security may be very important and vital for some business areas. A standard floor plan of a security-conscious shared working area is shown in Figure 3.6. This area is used for various purposes by people with specific roles, which could need different degrees in security access. If the need for security is listed through this field of work; it can be said that Commander Office needs stricter security requirements than General Operations Space. On the other hand, Secure Files, have a stricter security requirement. If the connections in the workplace are provided by WiFi, due to the wide spread of WiFi signals, everyone on the floor can access this connection, which may not meet the security needs of people with specific job descriptions. This hierarchical need for security can be met with LiFi. Each circle in Figure 3.3 represents a LiFi access point. In contrast to the WiFi access point, each of these LiFi access points provides wireless connection to a certain person or desk. The security of different rooms, for example between Secure Files and General Operations Area, can be provided with LiFi since the light cannot pass through the wall. Dual-gate locking can be used since light is contained in room. In this locking method, for access to that particular light, an additional luminaire-specific key may be needed and can be handover to

one of the near lights. In the diagram, there are some circles colored as green and red. Green circles are called fences. These fences prevent unauthorized users from infiltrating this boundary in other words this allows access to the devices connected inside the fence to be physically restricted if someone sitting outside the fence does not have the correct level of security.

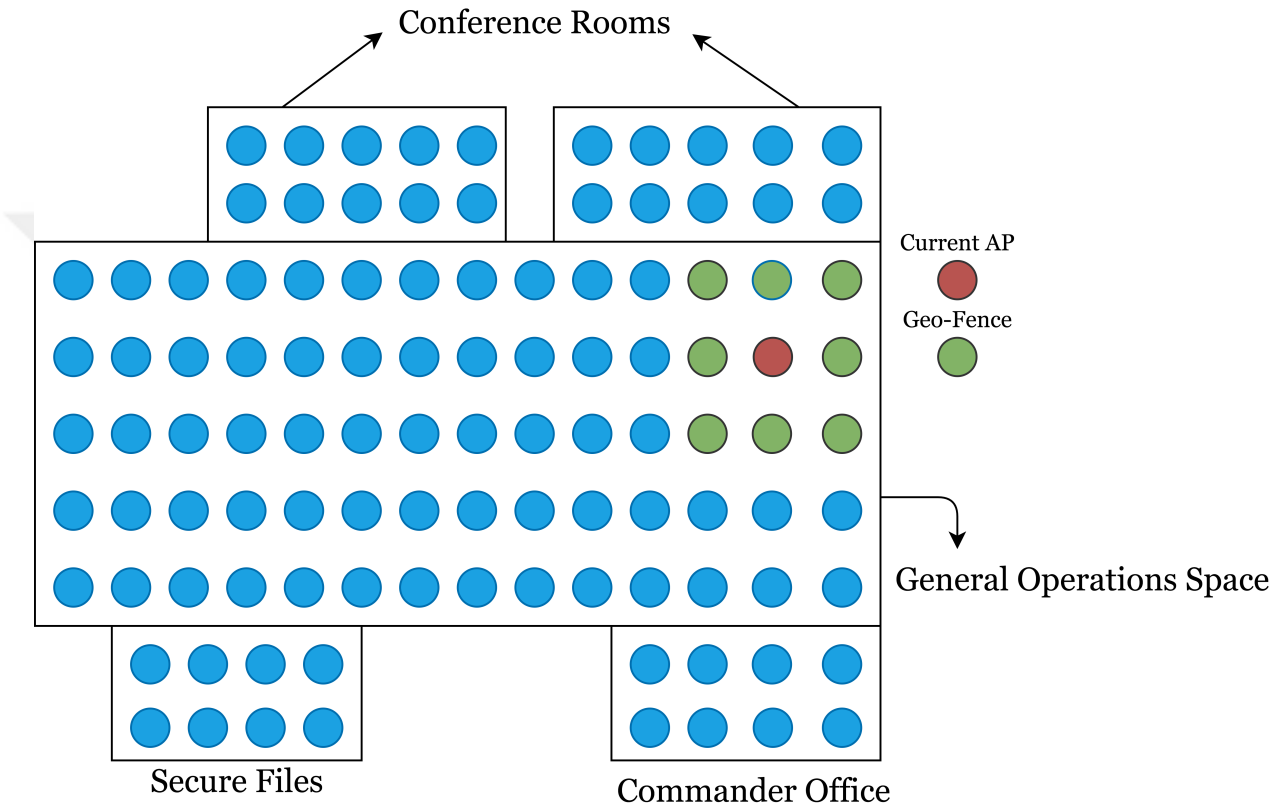

Figure 3.6 Geo-fencing

4. PHYSICAL LAYER SECURITY WITH OGSSK

In this section, some of our recent research results are presented the PLS problem with a promising new modulation technique [25]. A PLS algorithm based on OGSSK is proposed and its operation is briefly explained.

The OGSSK is a novel MIMO technique, which activates only certain number of LEDs for transmission at any time instant and uses the indices of those active LEDs to implicitly convey information. It differs from the concept of spatial modulation (SM) in terms of the absence of symbol information transmission, which greatly simplifies the complexity of VLC detection in OGSSK and also provides almost the same performance gains.

It is assumed that the user is connected to a single optical wireless communication (OWC) attocell with N_t LEDs and equipped with N_r ($N_r < N_t$) PDs as the receiver unit. In OGSSK, since multiple LEDs remain active (in this works it is assumed N_a) to send information through their index, combinations of a number of possible LEDs that can be created and used as spatial constellation points is $\binom{N_t}{N_a}$. The number of N_a combinations that can be considered for activation must be power of the two. That is, only $M_a = 2^{m_a}$ combinations are randomly selected and used to activate the selected LEDs, where, $m_a = \lfloor \log_2 \binom{N_t}{N_a} \rfloor$, here $\lfloor . \rfloor$ is the floor operation. m_a is the number of bits that can be transmitted using OGSSK, accordingly, the total spectral efficiency of the system in bits per channel use (bpcu) is $\eta = \log_2(M_a)$. d=(d1,d2,..) is a random array of independent data bits, these bits enters an OGSSK mapper, where m_a bit groups are mapped to an constellation point vector $x = [x_1, x_2, \cdots, x_{N_t}]^T$. During the optical transmission, since N_a LED is active only N_a

of the x_j's in x will be nonzero. For $I = 1, 2, \cdots, M_a$, $\mathbf{x}$ has the following form;

$$\mathbf{x}_I = \begin{bmatrix} 0 & P_1 & \cdots & 0 & P_2 & 0 \cdots & P_{N_a} & 0 \\ & \uparrow & & & \uparrow & & \uparrow & \\ & i_1^{th} \text{ pos.} & & & i_2^{th} \text{ pos.} & & i_{N_a}^{th} \text{ pos.} & \end{bmatrix}^T, \tag{4.1}$$

where, $I \Leftrightarrow \{i_1, i_2, \cdots, i_{N_a}\}$ and P_k represents positive and real-valued signal component that is transmitted by the i_kth activated LED. The possible values of signals, P_k, for $k = 1, 2, \cdots, N_a$ will be determined during the pre-equalization and precoding at transmitter.

$\mathbf{P} = [P_1, P_2, \cdots, P_{N_a}]^T$ represents the modulated signal vector. This vector's components are in the form of light intensities and transmitted through an optical channel $\mathbf{H} = [\mathbf{h}_1, \mathbf{h}_2, \cdots, \mathbf{h}_{N_t}] \in \mathbf{R}^+_{N_r \times N_t}$, where, $\mathbf{h}_k = [h_k(1), h_k(2), \cdots, h_k(N_r)]^T$.

In the following equation, $\mathbf{w}$ denotes an N_r-dim vector, its components are sum of the receiver thermal noise and shot noise caused by ambient light, which can be modelled as independent and identically distributed white Gaussian noise (AWGN) with double sided power spectral density σ^2 is added to the received signal. So, the received electrical signal at the receiver PD is given as follows:

$$\begin{aligned} \mathbf{y} &= \mathbf{H}\mathbf{x}_I + \mathbf{w} \\ &= \beta \mathbf{h}_{I,\text{eff}} + \mathbf{w} \end{aligned} \tag{4.2}$$

Here, $\mathbf{h}_{I,\text{eff}}$ can be expressed as $\mathbf{h}_{I,\text{eff}} = \sum_{k=1}^{N_a} \mathbf{h}_{i_k} P_k$ and it is called as "effective column vector" and β is a normalizing constant.

On the receiver side, the LED indices I used during transmission is estimated by OGSSK detectors (PDs) and demaps the symbol to the component bits accordingly. Maximum likelihood (ML) detector is used to detect LED indices.

$$\begin{aligned} \widehat{I} &= \arg\min_I p(\mathbf{y}|\mathbf{x}_I, \mathbf{H}) \\ &= \arg\min_I \parallel \mathbf{y} - \beta \mathbf{H}_I \mathbf{P} \parallel^2 \end{aligned} \tag{4.3}$$

where the estimated LED indices are denoted by $\widehat{I} \in \{1, 2, \cdots, M_a\}$ and $\mathbf{H}_I$ is obtained from $\mathbf{H}$ as

$$\mathbf{H}_I = \begin{bmatrix} h_{1,i_1} & h_{1,i_2} & \cdots & h_{1,i_{N_a}} \\ h_{2,i_1} & h_{2,i_2} & \cdots & h_{2,i_{N_a}} \\ \vdots & \ddots & \ddots & \\ h_{N_r,i_1} & h_{N_r,i_2} & \cdots & h_{N_r,i_{N_a}} \end{bmatrix} \in \mathcal{R}^{N_r \times N_a}. \tag{4.4}$$

4.1 OGSSK Based PLS Technique for Indoor VLC

The block diagram of the proposed PLS technique for OGSSK is shown in Figure 4.1. As seen in this diagram, a proper pre-equalizer and pre-coder should be designed. In the following subsection, design of the pre-equalizer and pre-coder will be explained briefly.

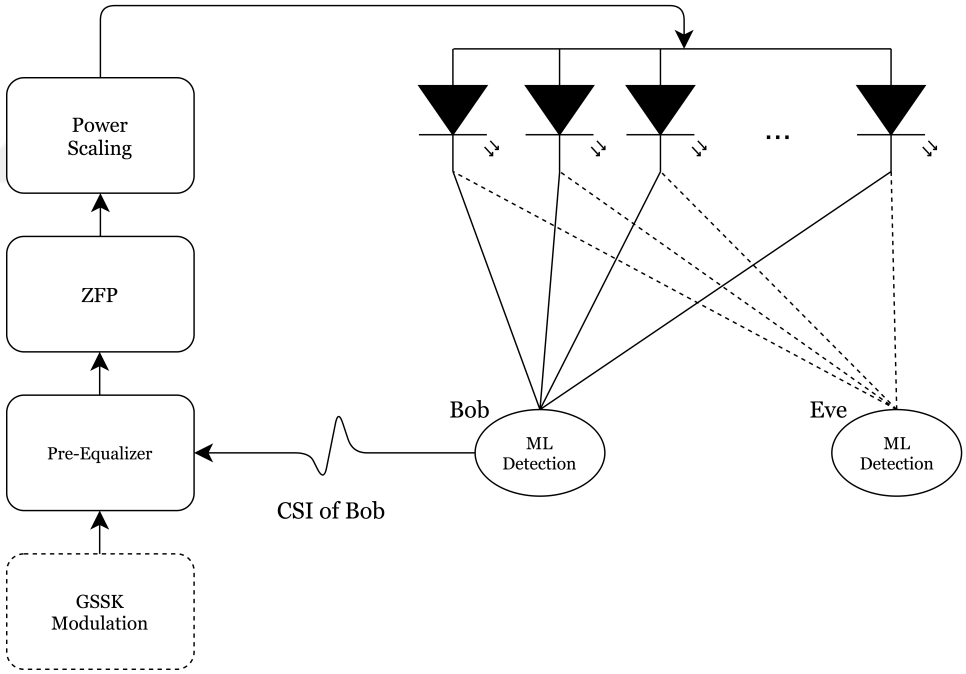

Figure 4.1 Block diagram of proposed PLS technique for OGSSK

4.1.1 Design of Pre-equalizer

Using the Bob's channel state information (CSI), the proposed pre-equalizer is designed. This pre-equalizer mainly shapes the original channel effective column

vectors, which are $\mathbf{H}_{\text{eff}} = [\mathbf{h}_{1,\text{eff}}, \cdots, \mathbf{h}_{M_a,\text{eff}}] \in \mathcal{R}^{N_r \times M_a}$, scattered in N_r-dim Euclidean space so that they are separated from each other at the maximum level. Suppose that for a given N_t and N_r ($N_t > N_r$), N_a, the number of active LEDs of the legitimate user (Bob), is greater than or equal to the number of PDs in the receiving unit. So, $N_a \geq N_r$. This assumption allows us to design the pre-encoder to ensure that there are no energy leaks between the different PDs in the receiver unit.

Pre-equalized $M_a (M_a \leq M)$ effective channel column vectors in

$$\widetilde{\mathbf{H}}_{\text{eff}} = [\widetilde{\mathbf{h}}_{1,\text{eff}}, \widetilde{\mathbf{h}}_{2,\text{eff}}, \cdots, \widetilde{\mathbf{h}}_{M_a,\text{eff}}] \in \mathcal{R}^{N_r \times M_a}$$

are chosen from the set of vector $\mathcal{V}_{M-\text{GQAM}} = \{\mathbf{v}_1, \mathbf{v}_2, \cdots, \mathbf{v}_M\}$, in an N_r-dim Euclidean space, forming an M-ary generalized quadrature-amplitude modulated (M-GQAM) signal constellation,

$$\mathbf{v}_k = [v_k(1), v_k(2), \cdots, v_k(N_r)]^T \in \mathcal{R}^{N_r}$$

where $k = 1, 2, \cdots, M$, and $v_k(\ell) \in \{\pm A, \pm 3A, \cdots, \pm(L-1)A\}$. Here, $M = L^{N_r}$, for $L = 2, 4, 6, \cdots$, and $A > 0$ denotes a real normalizing constant, whose value is determined during the following step which is precoding.

It can be shown that, for a given M_a and N_r, the size, M of the GQAM constellation can be determined as follows.

$$M = \begin{cases} M_a; & \text{if } N_r = 1 \\ \left(2\lceil \frac{1}{2} M_a^{1/N_r} \rceil\right)^{N_r}; & \text{if } N_r > 1 \end{cases} \tag{4.5}$$

where $\lceil . \rceil$ denotes ceiling operation. In Table 4.1, the M values for given M_a and N_r are shown.

After pre-equalization, the array of information bits to be transmitted by the OGSSK technique is mapped with the constellation vector $\mathbf{x}$, which indicates activated LEDs. At the output of the pre-equalizer $P_1, P_2, \cdots, P_{N_a}$, are obtained. These values generally take positive and negative real values. This can also be handled by adding a

Table 4.1 Size of Signal Constellations

M_a	$N_r = 1$ M-ary PAM	$N_r = 2$ M-ary QAM	$N_r = 3$ M-ary GQAM
2	2	4	Not feasible
4	4	4	8
8	8	16	8
16	16	16	64
32	32	36	64
16	16	16	64
64	64	64	64
16	16	16	64
128	128	144	216
256	256	256	512

suitable DC(direct current) component to each LED in the transmission unit. To meet the positivity constraint, the signals received in each kth PD after propagation through the optical channel have terms representing interference or energy leaks from the other LEDs labeled $i_j,\ j = 1, 2 \cdots, N_a (j \neq k)$. As shown in Figure 4.1, to ensure that there are no energy leaks in the PD outputs and to work within the physical operating range of the LEDs where fluctuations caused by the precoding process are reduced a zero-forcing precoding (ZFP) is used.

4.1.2 Design of Precoder

The signal received at the outputs of the PDs without any leakage between the PDs should be proportional to the $\beta\widetilde{\mathbf{h}}_{I,\text{eff}}$ + noise the vector. Here, $\mathbf{h}_{I,\text{eff}} = [\widetilde{h}_{I,\text{eff}}(1), \widetilde{h}_{I,\text{eff}}(2), \cdots, \widetilde{h}_{I,\text{eff}}(N_r)]^T$, $I \in \{1, 2, \cdots, M_a\}$. In order to meet this requirement, a pre-coder design is made on the transmitter side. The designed pre-coder has inputs $\widetilde{\mathbf{H}}_{\text{eff}} \in \mathcal{R}^{N_r \times M_a}, \mathbf{H} \in \mathcal{R}^{N_r \times N_t}$ and I and output $\mathbf{P} = [P_1, P_2, \cdots, P_{N_a}]^T$. As a result, the optimal precoding vector $\mathbf{P}_{\text{opt}}$ is determined as follows. To prevent

energy leakage in transmission, it must be like

$$\mathbf{H}_I\mathbf{P} = \widetilde{\mathbf{h}}_{I,\text{eff}} \tag{4.6}$$

$\mathbf{H}_I \in \mathcal{R}^{N_r \times Na}$ is given before (4.4). $(\mathbf{H}_I^T\mathbf{H}_I)^{-1}$ matrix specified here, is a non-singular matrix, to find the optimal precoding vector, the general inverse of $\mathbf{H}_I$ is taken, as

$$\mathbf{P}_{\text{opt}} = \left(\mathbf{H}_I^T\mathbf{H}_I\right)^{-1}\mathbf{H}_I^T\widetilde{\mathbf{h}}_{I,\text{eff}}. \tag{4.7}$$

Since $\mathbf{H}_I\left(\mathbf{H}_I^T\mathbf{H}_I\right)^{-1}\mathbf{H}_I^T \in \mathcal{R}^{N_r \times Nr}$ is a unit diagonal matrix, it can be written as

$$\mathbf{H}_I\mathbf{P}_{\text{opt}} = \mathbf{H}_I\left(\mathbf{H}_I^T\mathbf{H}_I\right)^{-1}\mathbf{H}_I^T\widetilde{\mathbf{h}}_{I,\text{eff}} = \widetilde{\mathbf{h}}_{I,\text{eff}}. \tag{4.8}$$

Then, both side are multiplied by $\mathbf{H}_I^T$ to show $\mathbf{U} \triangleq \mathbf{H}_I\left(\mathbf{H}_I^T\mathbf{H}_I\right)^{-1}\mathbf{H}_I^T$ is an unit matrix. That is, $\mathbf{H}_I^T\mathbf{U} = \mathbf{H}_I^T$. To ensure this equality, $\mathbf{U} \equiv \mathbf{I}_{N_r}$, where $\mathbf{I}_{N_r} \in \mathcal{R}^{N_r \times Nr}$ is an unit matrix.

Since $\mathbf{H}_I \in \mathcal{R}^{N_r \times Na}$ in (4.1) has more columns than rows ($N_a \geq N_r$), the matrix $\mathbf{H}_I^T\mathbf{H}_I$ in (4.12) is positive semi-definite and so (4.11) may not have a unique solution. For this reason, the standard trick is used, which slightly disrupts $\mathbf{H}_I^T\mathbf{H}_I$, to be positive precise. As a result, the final form of the optimal precoding vector

$$\mathbf{P}_{\text{opt}} = \left(\mathbf{H}_I^T\mathbf{H}_I + \epsilon\mathbf{I}_{N_a}\right)^{-1}\mathbf{H}_I^T\widetilde{\mathbf{h}}_{I,\text{eff}}, \tag{4.9}$$

Adding a small amount of identity matrix with $\epsilon > 0$ here guarantees its invertibility. As a general rule, ϵ must be selected to meet $\epsilon < \lambda_{\min},$; where $\lambda_{\min}$ represents the smallest non-zero eigenvalue of the $\mathbf{H}_I^T\mathbf{H}_I$ matrix.

4.1.3 Normalization of Powers at Transmitter

The signal components of $\mathbf{P}_{\text{opt}}$, denoted as $P_{k,\text{opt}}$, that signal components arriving each LED are real-valued variables that take $[-P_{\max}, P_{\max}]$ values with significant power fluctuations and a wide dynamic range. For $k = 1, 2, \cdots, N_a$, the normalized signal power $\overline{P}_k$, are subject to a power constraint for each luminary. This power constraint is $|\overline{P}_k - P_{dc}| \leq \alpha P_{\text{dc}}$, where P_{dc} is a dc(direct current) bias and $\alpha \in [0, 1]$

is a constant selected so that the linearity is maintained over the LED operating range $[(1-\alpha)P_{\mathrm{dc}}, (1+\alpha)P_{\mathrm{dc}}]$

As a result, signal driving kth LED which the peak constrained are determined as follows:

$$\overline{P}_k = \begin{cases} \beta P_{k,\mathrm{opt}} + b, & \text{if } k \in I \\ b & \text{if } k \notin I \end{cases} \tag{4.10}$$

where $\beta = \alpha P_{\mathrm{dc}}/P_{\max}$ and $b = P_{dc}$.

The transmitted signal at the receiver and eavesdropper side as follows:

$$y_B = \mathbf{h}_B^T \mathbf{x}_I + w_B \tag{4.11}$$

$$y_E = \mathbf{h}_E^T \mathbf{x}_I + J_B + w_E \tag{4.12}$$

In this equations (4.11)(4.12), w_B and w_E are denote noise components which have zero mean and variances σ_B^2 and σ_E^2, respectively. x_I is the modulated signal which is given in (4.1). J_B represents the jamming signal and it can be expressed as;

$$J_B = \beta(\mathbf{h}_E^T - \mathbf{h}_B^T)\mathbf{x}_I \tag{4.13}$$

Eavesdropper also receives an additional jamming signal so that the original message cannot be received in a meaningful way.

Maximum likelihood (ML) detector is used at transmitter and eavesdropper side to detect LED indices.

.

$$\hat{I}_{K,B} = \arg\min_{I_K} \left\{ ||y_B - s_B||^2 \right\}, \tag{4.14}$$

$$\hat{I}_{K,E} = \arg\min_{I_K} \left\{ ||y_E - s_E||^2 \right\}, \tag{4.15}$$

Here, s_B and s_E can be expressed as follows;

$$s_B = \mathbf{h}_B^T \mathbf{x}_I \tag{4.16}$$

$$s_E = \mathbf{h}_E^T \mathbf{x}_I \tag{4.17}$$

The detection process here is directly related to y_E. Therefore, it is clear that the detection depends on the estimation of the β.

4.1.4 ML Estimations of β

From the observation equation (4.11) at receiver, for a given pilot symbol $\mathbf{x} = \mathbf{s}_p$ $\left(\mathbf{s}_p \text{ are chosen from } \{\widetilde{\mathbf{h}}_{I,\text{eff}}\} \text{ for } I = 1, 2, \cdots N_a\right)$, the conditional probability density function (pdf) $\mathbf{y}_B$, given β can be expressed as

$$p(\mathbf{y}_B|\beta) \sim \exp\left(-\frac{1}{2\sigma_{\text{w}}^2}|\mathbf{y}_B - \beta\mathbf{s}_p|^2\right), \quad p = 1, 2, \cdots, P. \tag{4.18}$$

Maximizing (4.11) with respect to β, the ML estimate of β can be obtained as

$$\widehat{\beta}_{ML} = \frac{\mathbf{y}_B^T \mathbf{s}_p}{||\mathbf{s}_p||^2}. \tag{4.19}$$

4.2 Achievable Secrecy Capacity Bounds

Now in order to validate our research result we need to compute secrecy capacity. However, Secrecy capacity is not possible to compute exactly, hence some upper and lower bounds need to be found for it. In an OGSSK-based VLC system, lower and upper bounds of secrecy capacity can be expressed as follows [25]:

$$C_{\text{GSSK}} \leq \frac{N_r}{2}\log_2\left(\frac{\det(\text{C}_{\text{w}})^{1/N_r}}{\sigma_{\text{B}}^2}\right) - \zeta_{\text{U}} \tag{4.20}$$

$$C_{\text{GSSK}} \geq \frac{N_r}{2}\log_2\left(\frac{\det(\text{C}_{\text{w}})^{1/N_r}}{\sigma_{\text{B}}^2}\right) - \zeta_{\text{L}} \tag{4.21}$$

Here, ζ_U and ζ_L can be shown as;

$$\zeta_{\text{U}} = \frac{N_r}{2}\log_2\left(\frac{\exp(1)\det\left(\text{D}_{\text{w}}\right)^{1/N_r}}{2\sigma_{\text{B}}^2}\right) - \log_2(K) + \log_2\left(1 + (K-1)\exp\left(-\frac{\rho^2}{4\sigma_{\text{B}}^2}d_{\text{min}}^2\right)\right) \tag{4.22}$$

$$\zeta_{\text{L}} = \frac{N_r}{2}\log_2\left(1 + \frac{\det(\text{C}_{\text{w}} - \sigma_{\text{B}}^2\text{I}_{N_r})^{1/N_r}}{\sigma_{\text{B}}^2 K^{(2/N_r)}}\right) \tag{4.23}$$

where, $\text{D}_{\text{w}} = \text{diag}(\text{C}_{\text{w}})$.

4.3 Simulation Results

In this section, simulation results for the proposed OGSSK based indoor VLC physical security system are presented. Computer results are show BER performances for legitimate users and eavesdroppers, for different scenarios on different locations and geometry of the luminaries on the ceiling, as well as the different positions of the user and the number of receivers and the eavesdropper on the floor. In the simulation setups given below, each fixture surrounds 7 LEDs located around the fixture, and 1 W optical power radiates by each LED. The half-power semi angle of each LED is 60^o. The configurations of each PD's field of view (FoV) assumed to be 70^o and physical areas of these PDs are assumed to be 1 cm^2. The reflectance coefficients of the floor and walls materials are determined as 0.3 and 0.8, respectively.

As shown in the Figure 4.2, a $5 \times 5 \times 3$ m^3 room is considered and there are 8 uniformly distributed fixtures on the ceiling of the room to illuminate this room. That is, $N_t = 8$. Locations of these fixtures are given as;

$$\mathbf{p}_{\text{tx}} = \begin{bmatrix} 1.5 & 1.5 & 1.5 & 1.5 & -1.5 & -1.5 & -1.5 & -1.5 \\ -2.25 & -0.75 & 0.75 & 2.25 & -2.25 & -0.75 & 0.75 & 2.25 \end{bmatrix}. \tag{4.24}$$

In these computer simulations, it is assumed that each receiver is equipped with 2 PDs placed at a height of 0.85 m and separated by a distance of 3 cm. These simulation studies were carried out for three different scenarios, as shown in Figure 4.2. Depending on the locations of the users and their distance from each other, simulation results were obtained through the scenarios as below.

***Scenario 1*:** In the indoor geometry shown in Figure 4.2 (a), the locations of the receivers are selected as $[-2.2], [2, -2]$ meters. The MIMO channel matrix for receiver Bob and Eve are given below.

$$\mathbf{H}_{\text{B}} = 10^{-5} \times \begin{bmatrix} 6.6036 & 4.0374 & 1.5469 & 1.0099 & 1.0919 & 1.0458 & 0.8438 & 0.72101 \\ 7.4745 & 4.4703 & 1.6317 & 1.0434 & 1.2341 & 1.1560 & 0.8926 & 0.7500 \end{bmatrix}.$$

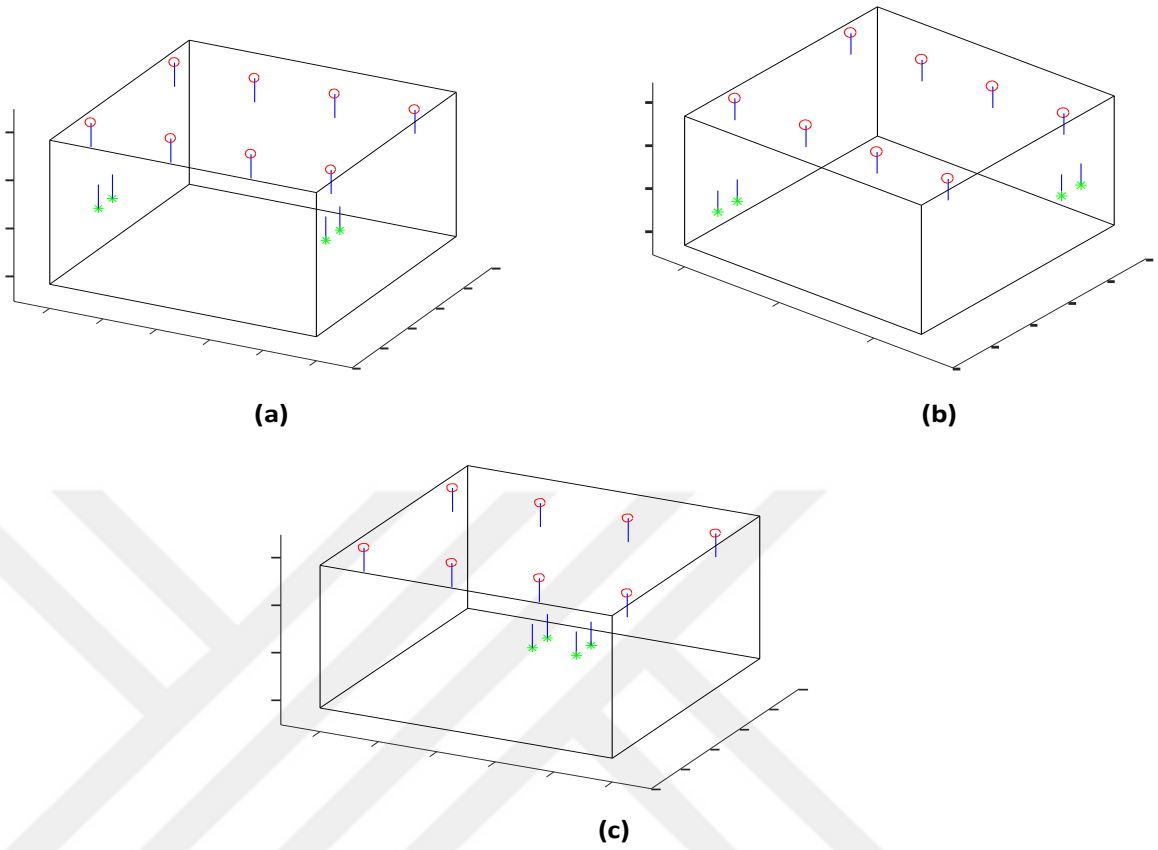

Figure 4.2 Transmission geometry for the scenarios. Transmitter locations: red circles, location of PD on receiver: green asterisk and element orientation: blue segment.

$$\mathbf{H}_{\mathrm{E}} = 10^{-5} \times \begin{bmatrix} 0.7355 & 0.8699 & 1.1410 & 1.2275 & 1.0433 & 1.6269 & 4.4093 & 7.46671 \\ 0.7159 & 0.8307 & 1.0418 & 1.0930 & 1.0012 & 1.5440 & 4.0112 & 6.5833 \end{bmatrix}.$$

***Scenario 2*:** In the indoor geometry shown in Figure 4.2 (b), the locations of the receivers are selected as $[-2.5, -0.5], [1.5, 0]$ meters. The MIMO channel matrix for receiver Bob and Eve are given below.

$$\mathbf{H}_{\mathrm{B}} = 10^{-5} \times \begin{bmatrix} 2.3909 & 1.3824 & 0.6885 & 0.4763 & 3.4712 & 1.7520 & 0.7627 & 0.5051 \\ 1.6461 & 1.0828 & 0.6166 & 0.4454 & 4.7690 & 2.1299 & 0.8271 & 0.5291 \end{bmatrix}.$$

$$\mathbf{H}_{\mathrm{E}} = 10^{-5} \times \begin{bmatrix} 1.1441 & 1.7189 & 3.5014 & 4.0126 & 1.0660 & 1.4846 & 2.5946 & 2.8974 \\ 1.0657 & 1.4845 & 2.5963 & 2.8992 & 1.1448 & 1.7188 & 3.5021 & 4.0142 \end{bmatrix}.$$

***Scenario 3*:** In the indoor geometry shown in Figure 4.2 (c), the locations of the receivers are selected as $[-2.5, -0.5], [1.5, 0]$ meters. The MIMO channel matrix for receiver Bob and Eve are given below.

$$\mathbf{H}_{\mathrm{B}} = 10^{-5} \times \begin{bmatrix} 2.0514 & 3.3091 & 3.3086 & 2.0510 & 1.7306 & 2.4587 & 2.4610 & 1.73181 \\ 1.7305 & 2.4602 & 2.4602 & 1.7306 & 2.0529 & 3.3086 & 3.3110 & 2.0552 \end{bmatrix}.$$

$$\mathbf{H}_{\mathrm{E}} = 10^{-5} \times \begin{bmatrix} 1.4627 & 2.4004 & 3.8357 & 2.9738 & 1.3101 & 1.9238 & 2.7576 & 2.3225 \\ 1.3101 & 1.9253 & 2.7579 & 2.3202 & 1.4635 & 2.4001 & 3.8371 & 2.9795 \end{bmatrix}.$$

In Figure 4.3, it is shown that the average BER performance vs. SNR for each scenarios which are given above. When the simulation results obtained are examined; for example, when the BER performances of both users (Bob and Eve) at SNR values around 25 dB Bob's BER performances reaches 10^{-4}, while Eve's performance could not exceed 3×10^{-1} on a similar SNR scale.

In this computer simulations have shown that the proposed PLS algorithm performs very well when the user's channel is perfectly known. In this thesis, the performance of the proposed algorithm will be shown assuming that the channel is estimated, that is, imperfect CSI.

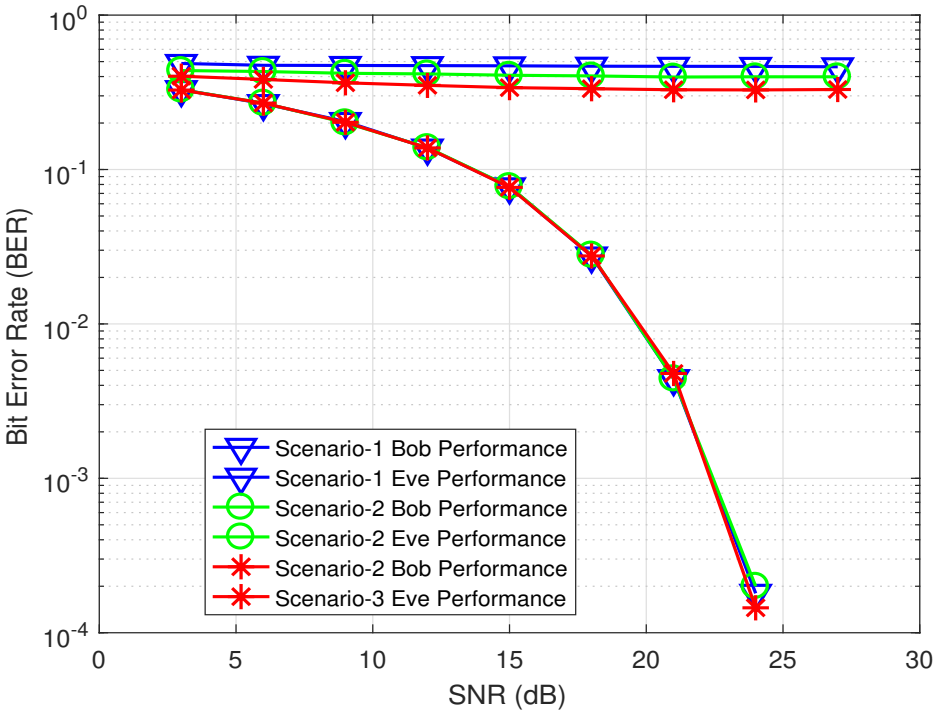

Figure 4.3 BER vs. SNR performances for Bob and Eve in an OGSSK-based VLC system

5. CHANNEL ESTIMATION IN VISIBLE LIGHT COMMUNICATIONS SYSTEMS

As seen in the physical layer security algorithm in OGSSK based systems that are described in detail and the simulation results are presented in the previous section, the security algorithm that is operated at the transmitter side, needs to employ the channel state information (CSI). This information should be obtained by any suitable channel estimation techniques.

In this section, an efficient channel estimation technique for DCO-OFDM based

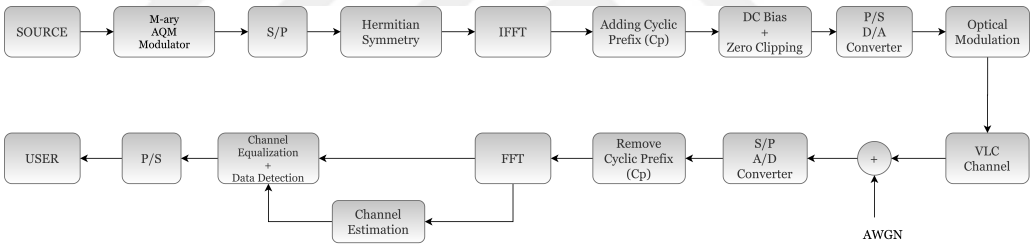

Figure 5.1 Block Diagram of a DCO-OFDM System

VLC systems in the presence of clipping noise will be presented.

5.1 System Model

In the DCO-OFDM system with N subcarriers, a DC bias is added to the signal to make it positive and, therefore, all the OFDM subcarriers carry data symbols. At the transmitter these subcarriers are assumed to be actively employed to transmit data symbols modulated by either M-level quadrature amplitude modulation (M-QAM) or phase shift keying (M-PSK). Frequency domain complex-valued vector of data symbols $\mathbf{X} = [X[0], X[1], \cdots, X[N-1]]^T$ meets the Hermitian symmetry and the components at the 0th (DC) and $(N/2)$th subcarriers are set to zero as follows

[33],

$$X[k] = \begin{cases} 0, & \text{if } k = 0 \\ X^*[N-k], & \text{if } k = 1, 2, \cdots, (N/2)-1 \\ 0, & \text{if } k = N/2 \end{cases} \tag{5.1}$$

where $(*)$ denotes the complex conjugation. Consequently, time-domain signal samples obtained at the output of the fast Fourier transform ($\mathcal{FFT}$) become real-valued due to the Hermitian symmetry [33]. The resulting real, bipolar and anti-symmetric time-domain signal vector $\mathbf{x} = [x[0], x[1], \cdots, x[N-1]]^T$ is denoted as

$$x[n] = \sum_{k=1}^{N} X[k] e^{j2\pi kn/N} \tag{5.2}$$

where N is the number of points in the inverse Fourier transform ($\mathcal{IFFT}$) and $X[k]$ is the kth component of $\mathbf{X}$. Due to Hermitian symmetry and zero insertion process at the subcarriers $k = 0$ and $k = N/2$, the number of data symbols carried by the subcarriers in DCO-OFDM is only $N/2 - 1$. A cyclic prefix (CP) of length N_{cp} is then added to the discrete time samples. N_{cp} must be greater or equal to the maximum channel delay spread. In our simulations, N_{cp} is taken as $N_{cp} \geq L$. After digital-to-analog conversion the electrical signal, $x(t)$ is generated in analog form. Note that $x(t)$ can be modelled approximately as a Gaussian process due to the central limit theorem. It can be easily seen that its mean is zero and the variance can be determined by $\sigma_x^2 = E\{x^2(t)\}$. A suitable DC bias is next added to $x(t)$ and the residual negative peaks are clipped resulting in a signal denoted by $x_c(t)$. Note that since the peak to average ratio of the OFDM samples in the time-domain is substantially high, a large DC bias would be necessary to eliminate the negative part of $x(t)$. However, this increases the optical energy per bit, making the scheme quite inefficient in terms of the optical power. Therefore, instead, a moderate DC bias is employed in real applications and the residual negative signal components are clipped. However this will inevitably generate a *clipping noise* and based on the level of the clipping noise set by the designer, the BER performance of the scheme will be affected. Usually the DC bias level denoted by V_{DC} is determined by the standard deviation of $V_{DC} = \rho\sqrt{E\{x^2(t)\}}$, where ρ is a constant and to be

determined from $10\log(\rho^2+1)$ dB for a given distortion level in dB. Consequently, time-domain samples obtained at the $\mathcal{IFFT}$ output of the DCO-OFDM system with a DC component are dented by $\tilde{x}[n] = x[n] + V_{\mathrm{DC}},\ n = 0, 1, \cdots, N-1$. Hence, after the clipping process, these samples becomes strictly positive valued as

$$x_c[n] = \begin{cases} \tilde{x}[n] & \text{if } \tilde{x}[n] \geq 0 \\ 0 & \text{if } \tilde{x}[n] < 0 \end{cases} \tag{5.3}$$

where $e_c[n] = x_c[n] - \tilde{x}[n]$ represents the clipping noise sample. Note that, for a large number of subcarriers, the amplitude of the unclipped DCO-OFDM time-domain samples can be approximated by a Gaussian distribution. Thus, the amplitude distribution of the clipped signal samples, $x_c[n]$ has a half-Gaussian distribution as

$$p_{x_c[n]}(x) = Q\left(V_{\mathrm{DC}}/\sigma_x\right)\delta(x) + \frac{u(x)}{2\pi\sqrt{\sigma_x}} e^{-(x-V_{\mathrm{DC}})^2/2\sigma_x^2}$$

where $u(.)$ denotes unit step function and $Q(x) = (1/\sqrt{2\pi})\int_x^\infty e^{-t^{2/2}}$. Then, the average transmitted electrical power $P_{\mathrm{elec;DCO}}$ of the above clipped signal is given by

$$\begin{aligned} P_{\mathrm{elec;DCO}} &= E\{x_c^2\} = \int_{-infty}^{\infty} x^2 p_{x_c}(x)dx \\ &= \left(\sigma_x^2 + V_{\mathrm{DC}}^2\right)\left(1 - Q(V_{\mathrm{DC}}/2\sigma_x)\right) \\ &\quad + \left(\sigma_x V_{\mathrm{DC}}/\sqrt{2\pi}\right)\exp\left(-V_{\mathrm{DC}}^2/2\sigma_x^2\right) \end{aligned} \tag{5.4}$$

Since $x_c[n] = \tilde{x}[n] + e_c[n]$, the corrupted data symbols in frequency domain due to the clipping noise can be determined as follows:

$$\begin{aligned} \mathbf{X_c} &= \mathcal{FFT}\{\mathbf{x_c}\} \\ &= \mathcal{FFT}\{\tilde{\mathbf{x}} + \mathbf{e_c}\} \\ &= \tilde{\mathbf{X}} + \mathbf{E_c} \end{aligned}$$

where $\mathbf{E_c} = [E_c[0], E_c[1], \cdots, E_c[N-1]]^T$ represents the clipping noise vector in the frequency domain. By means of the Bussgang theorem [34], the received OFDM signal in the frequency domain can be expressed in matrix form as ,

$$\mathbf{Y} = \mathbf{H}\tilde{\mathbf{X}} + \mathbf{C} + \mathbf{W} \tag{5.5}$$

where $\mathbf{H} = \mathrm{diag}[H_0, H_1, \cdots, H_{N-1}]$ is the optical channel coefficient matrix in the frequency domain and $\tilde{\mathbf{X}} = \mathbf{X} + \mathbf{u}$ represents the N-dimensional DC-biased data

vector. $\mathbf{u} = [1, 0 \cdots, N-1]^T$ is the $\mathcal{FFT}$ of the DC component. Finally, $\mathbf{C} = \mathbf{HE}_c$ and $\mathbf{W}$ represent the clipping noise vector and the additive white Gaussian noise vector with zero mean and variance σ_w^2, respectively. Note that (5.5), can be expressed in terms of the L-dim, discrete-time channel impulse response (IR) vector $\mathbf{h}$ as

$$\mathbf{Y} = \mathbf{Ah} + \mathbf{C} + \mathbf{W} \tag{5.6}$$

where $\mathbf{A} = \tilde{\mathbf{X}}\mathbf{F} \in \mathcal{C}^{N \times L}$, and $\mathbf{F} \in \mathcal{C}^{N \times N}$ denotes the Fourier transform matrix. Here, $\mathbf{h} \in \mathcal{R}^L$ represents the real-valued multi-path visible light channel IR whose nonzero elements are shown as $h_1, h_2, \ldots, h_L$, $(L << N)$. Note that, as it will be shown in the computer simulations section, because the electrical supply of the LEDs connected in series with a cable occurs with a time delay, the IR of the optical channel formed between the transmitter and the receiver appears in a sparse and frequency selective structure

5.2 Proposed Channel Estimation Technique

In this section, we propose an efficient sparse VLC channel estimation technique that also mitigate the effect of the clipping noise. Inspired by the work [35], the channel estimation algorithm is implemented in an iterative way. In each iteration step, the clipping noise samples are estimated by making use of the estimate of channel transfer function obtained in the previous estimation step. The details of the technique are given as follows: From (5.6), the matrix $\mathbf{A} \in C^{N \times L}$ can be written by the column vectors $\mathbf{A} = [\mathbf{a}_1, \mathbf{a}_2, \ldots, \mathbf{a}_L]$ as

$$\mathbf{Y} = \sum_{\ell=1}^{L} \mathbf{a}_{\eta_\ell} h_\ell + \mathbf{C} + \mathbf{W} \ , \tag{5.7}$$

where $\mathbf{h} = [h_1, h_2, \ldots, h_L]^T$, and $\eta = [\eta_1, \eta_2, \ldots, \eta_L]^T$, $\eta_1, \eta_2, \ldots, \eta_L \in \{1, 2, \ldots, N\}$, represent the channel path gains and the path delays, respectively. The components of the discrete frequency response of the sparse multi-path VLC channel, $\mathbf{H}$ can be expressed by

$$H_k = \sum_{\ell=0}^{L-1} h_\ell \exp\left(-j\frac{2\pi k \eta_\ell}{N}\right), \ k = 0, 1, \cdots, N-1. \tag{5.8}$$

The initial channel path gains and path delays are estimated by means of the equally spaced P pilot symbols, $X[i_p]$, each carried by the i_pth subcarrier for $p = 1, 2, \cdots, P$.

5.2.1 Estimation of Channel Path Delays and Path Gains

According to (5.5), the least squares (LS) estimates of the channel frequency response at the pilot subcarriers of the OFDM symbol, can be obtained as

$$\hat{H}_{i_p,i_p} = \frac{Y[i_p]}{X[i_p]} = H_{i_p,i_p} + Z[i_p] \tag{5.9}$$

where $Z[i_p] = \left(C[i_p] + W[i_p]\right)/X[i_p], \quad p = 1, 2, \cdots, P$. From (5.6) and (5.8), (5.9) can be expressed in vector form

$$\hat{\mathbf{H}}_p = \mathbf{\Psi}\mathbf{h} + \mathbf{Z} \tag{5.10}$$

where $\hat{\mathbf{H}}_p = [\hat{H}_{i_1,i_1}, \cdots, \hat{H}_{i_P,i_P}]^T$, $\mathbf{Z} = [Z_{i_1}, \cdots, Z_{i_P}]^T$ and $\mathbf{\Psi}$ is a $P \times L$ matrix whose (m, ℓ)'th element is $\Psi[m, \ell] = \exp\big(-j2\pi i_m \eta_\ell / N\big)$. We adopt a well known signal processing algorithm, called ESPRIT, to estimate the channel path delays from the channel correlation matrix, $\mathbf{R}_f = E\left\{\hat{\mathbf{H}}_p \hat{\mathbf{H}}^\dagger{}_p\right\}$. Away from CS-based algorithms, ESPRIT algorithm does not require *dictionary matrix* with any resolution order. Hence, the sparsity feature of the VLC channel can be exploited with a computational friendly algorithm. In general, $\mathbf{R}_f$ is unknown to the receiver but can be estimated first through spatial smoothing and then through time-averaging over few consecutive OFDM symbols $n = 0, 1, \cdots, M$ as $\bar{\mathbf{R}}_f = (1/M)\sum_{n=1}^{M} \hat{\mathbf{H}}_p(n)\hat{\mathbf{H}}^\dagger{}_p(n)$. Since the channel path delays and path gains do not change during several OFDM symbols in VLC channels, the averaging is performed perfectly. The ESPRIT algorithm uses the following steps:

- Perform an eigenvalue decomposition on $\bar{\mathbf{R}}_f$ as $\bar{\mathbf{R}}_f = \mathbf{U}\mathbf{\Sigma}\mathbf{U}^\dagger$, where $\mathbf{U} = [\mathbf{U}_s, \mathbf{U}_w]$ are the eigenvector matrices corresponding to the signal subspace and noise subspaces, and $\mathbf{\Sigma}_s, \mathbf{\Sigma}_w$ in

$$\mathbf{\Sigma} = \begin{bmatrix} \mathbf{\Sigma}_s & \mathbf{0} \\ \mathbf{0} & \mathbf{\Sigma}_w \end{bmatrix}$$

are the eigenvalue matrices corresponding to the signal and noise subspaces, respectively.

- Determine the $L \times L$ matrix $\mathbf{\Phi}$ by solving the (usually overdetermined) system of equations

$$\mathbf{U}_2 = \mathbf{U}_1 \mathbf{\Phi}, \tag{5.11}$$

where the $(N-1) \times L$ matrices $\mathbf{U}_1$ and $\mathbf{U}_2$, are constructed by the first $N-1$ and last $N-1$ rows of $\mathbf{U}_s$, respectively. The solution for $\mathbf{\Phi}$ can be obtained from (5.11) as $\widehat{\mathbf{\Phi}} = (\mathbf{U}_1^{\dagger}\mathbf{U}_1)^{-1}(\mathbf{U}_1^{\dagger}\mathbf{U}_2)$.

- Find an eigen-decomposition of the matrix $\widehat{\mathbf{\Phi}}$. It can be shown that $\widehat{\lambda}_\ell = e^{-j2\pi\tau_\ell/N}, \ell = 0, 1, \cdots, L-1$, where λ_ℓ is the ℓ^{th} eigenvalue of $\widehat{\mathbf{\Phi}}$.
- Determine the channel path delays as
$\widehat{\eta}_\ell = -\frac{N}{2\pi}\arg(\widehat{\lambda}_\ell),\ \ell = 0, 1, \cdots, L-1.$

Once the delays $\{\eta_\ell\}$ are estimated, the LS estimate of the channel path gains vector $\mathbf{h}$ is obtained as,

$$\widehat{\mathbf{h}} = \left(\widehat{\mathbf{\Psi}}^{\dagger}\widehat{\mathbf{\Psi}}\right)^{-1}\widehat{\mathbf{\Psi}}^{\dagger}\widehat{\mathbf{H}}_p. \tag{5.12}$$

where $\widehat{\mathbf{\Psi}}$ is the estimate of $\mathbf{\Psi}$ with, for $m = 0, \cdots, N-1;\ \ell = 0, \cdots, L-1$, $\widehat{\mathbf{\Psi}}[m, \ell] = \exp(-j2\pi i_m \widehat{\eta}_\ell / N)$

5.2.2 Iterative Channel Estimation Algorithm

We now propose an iterative channel estimation algorithm that is based on estimating the clipping noise in each iteration and compensating for its effect on the observed signal generated at the output of the $\mathcal{FFT}$ operation at the receiver. The initial channel estimate $\mathbf{H}^{(0)}$ is determined from the estimated channel impulse response by means of the pilot symbols, as explained in the previous section, as $\mathbf{H}^{(0)} = \mathbf{F}_L\widehat{\mathbf{h}}$, where $\mathbf{F}_L$ is an $N \times L$ DFT matrix. Following this step, data symbols are detected from (5.5) as

$$\mathbf{X}^{(0)} = \mathcal{DETECT}\left\{\left(\mathbf{H}^{(0)}\right)^{-1}\mathbf{Y}\right\} \tag{5.13}$$

from which the initial estimates of the transmitted OFDM time-domain samples are obtained by the $\mathcal{IFFF}$ operation as

$$\mathbf{x}^{(0)} = \mathcal{IFFT}\{\mathbf{X}^{(0)}\}$$

where $\mathcal{DETECT}\{a\}$ operator denotes a *hard decision* process. Then an initial estimate of the clipping noise is determined as

$$\mathbf{E}_c^{(0)} = \mathcal{FFT}\left\{\mathbf{x_c}^{(0)} - \tilde{\mathbf{x}}^{(0)}\right\}.$$

If $\mathbf{X}^{(0)} \approx \mathbf{X}$, BER is sufficiently small, then $\mathbf{E}_c^{(0)} \approx \mathbf{E}_c$. Under this condition, the estimates of the channel and the clipping noise, obtained in previous iteration can be used to get the next estimated values easily as follows:

Algorithm: Estimation of sparse VLC Channel in the Presence of Clipping Noise

Input: Observation vector:$\mathbf{Y}$, initial estimates: $\mathbf{H}^{(0)}$, $\mathbf{E}_c^{(0)}$

Output: Final estimated channel matrix $\mathbf{H}^{(N_{\text{iter}})}$

for $i = 1$ to N_{iter} **do**

$$\mathbf{Y} \implies \mathbf{Y} - \mathbf{H}^{(i-1)}\mathbf{E}_c^{(i-1)} \tag{5.14}$$

$$\mathcal{H} \equiv \left(\mathbf{X}^{(i-1)}\right)^{-1}\mathbf{Y} \tag{5.15}$$

$$\mathbf{h}^{(i)} = \left(\widehat{\mathbf{\Psi}}^{\dagger}\widehat{\mathbf{\Psi}}\right)^{-1}\widehat{\mathbf{\Psi}}^{\dagger}\mathcal{H} \tag{5.16}$$

$$\mathbf{H}^{(i)} = \mathbf{F}_L\mathbf{h}^{(i)} \tag{5.17}$$

$$\mathbf{X}^{(i)} = \mathcal{DETECT}\left\{\left(\mathbf{H}^{(i)}\right)^{-1}\mathbf{Y}\right\} \tag{5.18}$$

$$\mathbf{x}^{(i)} = \mathcal{IFFT}\{\mathbf{X}^{(i)}\} \tag{5.19}$$

$$\mathbf{E}_c^{(i)} = \mathcal{FFT}\left\{\mathbf{x_c}^{(i)} - \tilde{\mathbf{x}}^{(i)}\right\} \tag{5.20}$$

end for

In the following section, MSE and BER performances of the proposed iterative channel estimation algorithm for DCO-OFDM systems in the presence of clipping noise will be examined by computer simulations in relation to various clipping noise levels.

Table 5.1 Simulation Parameters

Number of subcarriers, N	1024
Bandwidth, BW	2 MHz
Samplng frequency, fs	1Ghz
Pilot symbols frequency	1/8
Multpath channel delay vector	η=[0 21 34 52]
Multipath channel gains [dB]	[S1, S2, S3, S4] [0.25 0.5 0.15 0.1]
Modulation	QPSK
Max iteration step, imax	3

5.3 Computer Simulations

The channel model considered in computer simulations is assumed to be formed as 4 LEDs, placed at the corners of a square with a certain edge length on the ceiling of a closed environment and a receiving photodiode placed at the base of the environment (Figure 5.2). As shown in Figures 5.3 and 5.4, the impulse response of the optical channel formed between the transmitter and the receiver of the system occurs in a sparse and frequency-selective structure, as the electrical supply of the LEDs connected in series with a cable causes a certain time delay. The system parameters for the simulation scenario considered are selected as in Table 5.1 and the proposed iterative channel estimation algorithm is used for estimating the coefficients and locations of the multi-path channel in a sparse structure. In the computer simulations, it is assumed that D/A converter and PD are ideal so that optical-to-electrical conversion constant ξ and electrical-to-optical conversion constant R are chosen as $\xi = R = 1$. Also we adopt using the transmitter transmit signal energy, $E_{b_{\text{elec;DCO}}}$ per additive Gaussian noise energy spectral density N_0 as a signal-to-noise ratio metric defined as [36]

$$\frac{E_{b_{\text{elec;DCO}}}}{N_0} = \frac{E\{x_c^2\}}{R_{\text{b,DCO}} N_0}.$$

It is seen that the least-square (LS) and the estimation of signal parameters via rotational invariant techniques (ESPRIT) algorithms employed for estimating the initial values of channel parameters greatly reduce the computational complexity.

In Figures 5.5 and 5.6, the MSE and SER performance curves of the channel estimation algorithm for quadrature phase shift keying (QPSK) modulation are obtained separately for the 2 dB level of clipping noise. From these curves, it is concluded that the proposed iterative algorithm contributes substantially to both MSE and BER performances of the system. In addition, it is observed that almost all of these contributions and gains are obtained during the 1st iteration; as a small increase is observed in the BER performance, the improvement in MSE performance becomes small enough to be neglected in the second iteration. Therefore, we conclude from these graphs that the nonlinear disturbance effects caused by clipping noise are greatly reduced by the proposed algorithm in a maximum of two iteration steps. However, it can be seen that the obtained BER performance curve does not converge to the BER curve when the channel is fully known, and also that the MSE performance does not converge to the MSE curve when all data symbols transmitted when the channel is perfectly known. This is mainly due to the fact that the time-domain samples at the OFDM output in the transmitter are clipped as a result of a nonlinear process. Similarly, the BER and MSE performances of the iterative channel estimation algorithm presented in Figures 5.7 and 5.8 are obtained when the clipping noise is $B = 1$ dB. It is seen from these graphs that similar results were obtained as the previous simulation results.

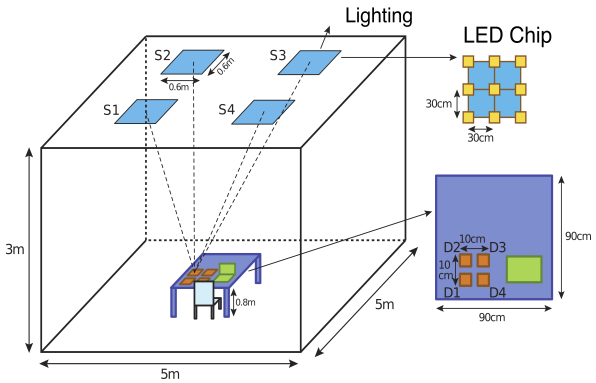

Figure 5.2 VLC channel model simulation environment

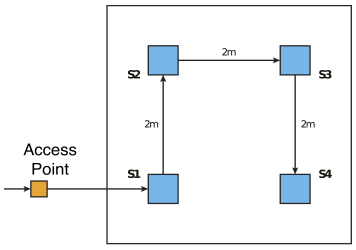

Figure 5.3 Realistic cabling topology (CAT-5)

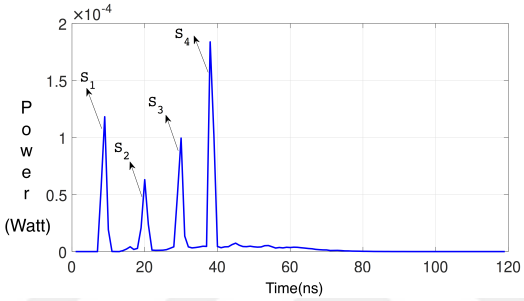

Figure 5.4 Channel impulse response due to delay in cabling

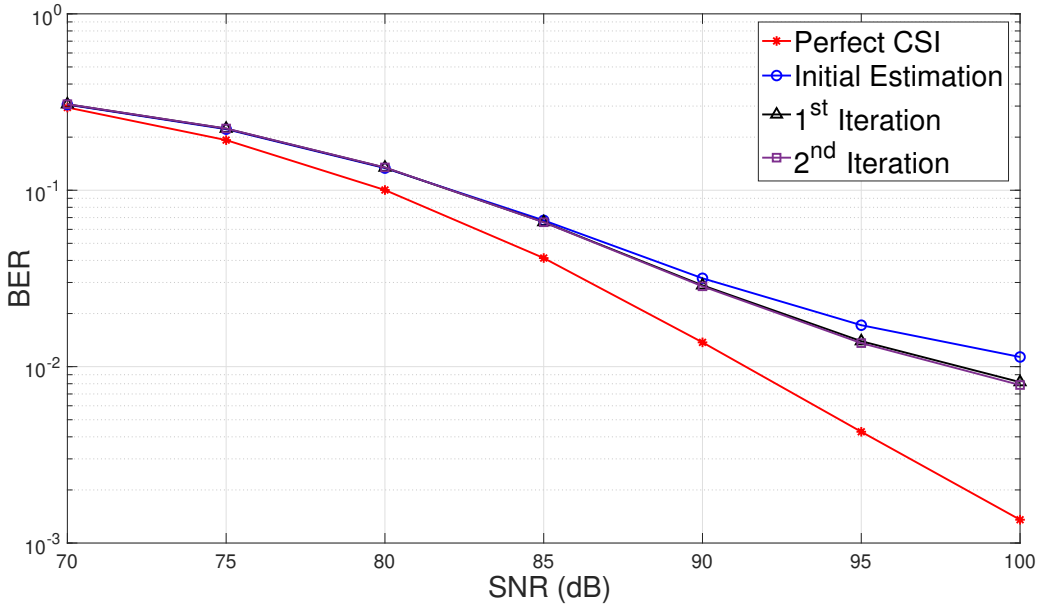

Figure 5.5 BER curve for $B = 2$dB

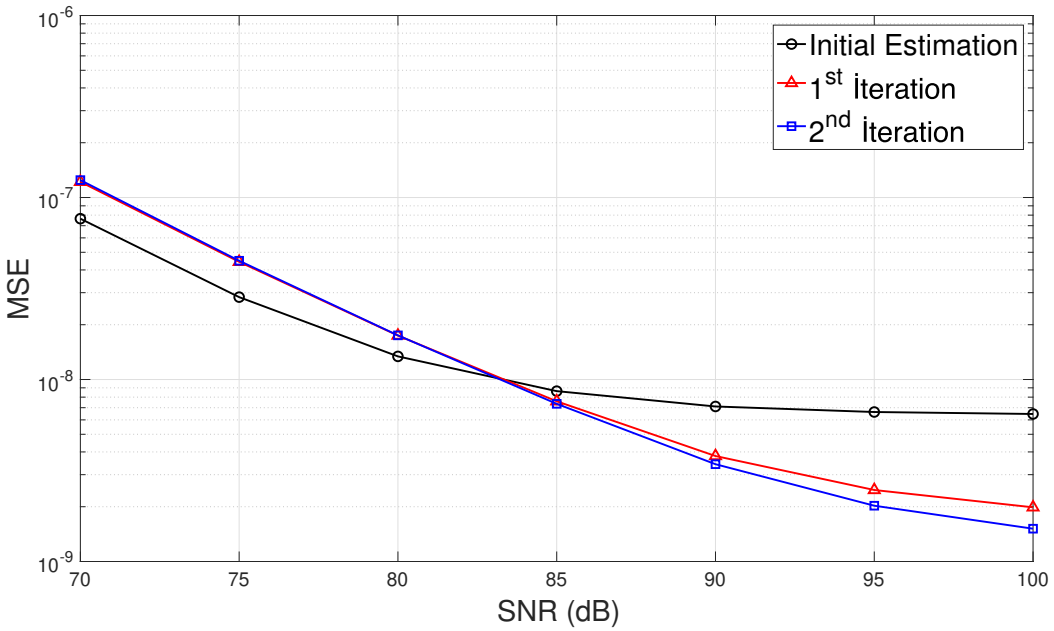

Figure 5.6 MSE curve for $B = 2$dB

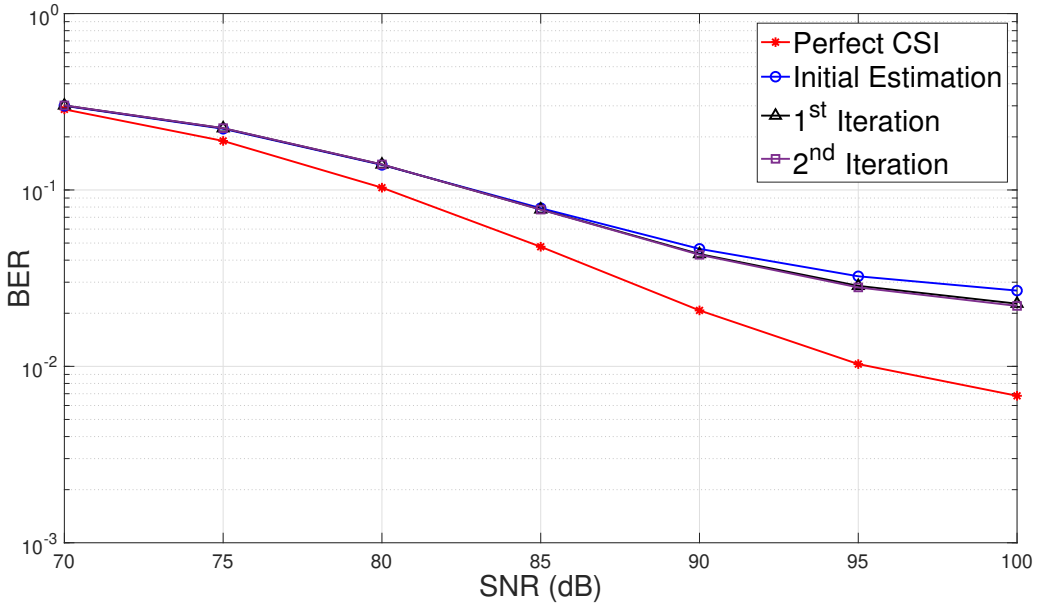

Figure 5.7 BER curve for $B = 1$dB

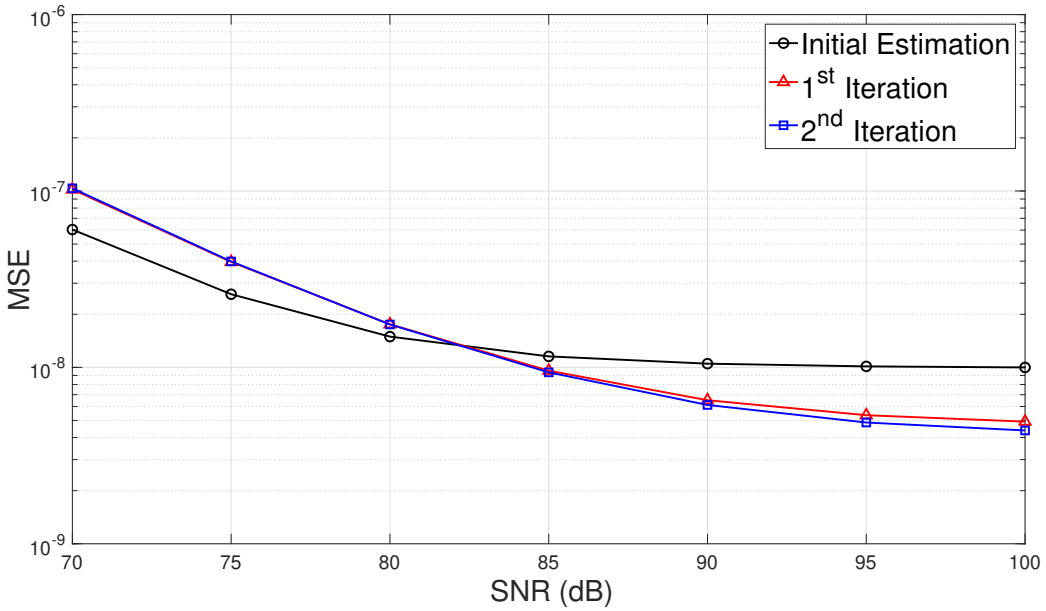

Figure 5.8 MSE curve for $B = 1\text{dB}$

6. VLC PHYSICAL-LAYER SECURITY WITH OGSSK IN THE PRESENCE OF IMPERFECT CSI

In previous chapters, we have shown that the proposed PLS algorithm for OGSSK based VLC systems had a very good BER performance in the presence of perfect CSI case. However, since the CSI cannot be known fully in real life applications, it is very important to analyze how sensitive this security algorithm developed to the channel estimation errors. In the following we present our investigations, analysis as well as the computer simulations results on this important issue.
Based on the results obtained in Section 4, the received signal by the legitimate user(Bob) can be expressed as:

$$\mathbf{y}_B = \beta \mathbf{G}\mathbf{x} + \mathbf{w}_B \tag{6.1}$$

where $\mathbf{G} \in \mathcal{R}^{N_r \times N_r}$ is defined as $\mathbf{G} = \mathbf{H}_I \mathbf{P}_{\text{opt}} = \mathbf{H}_I \left(\mathbf{H}_I^T \mathbf{H}_I\right)^{-1} \mathbf{H}_I^T$ and $\mathbf{x} = \widetilde{\mathbf{h}}_{I,\text{eff}}$ represents data symbol taking values from M-QAM signal constellation. β in (6.1) is a power scaling factor that fits the maximum value of the transmit signal within the linear dynamic range of the LEDs. As seen from the details presented in Sec. 4, the parameter β is related with the channel coefficients in a nonlinear fashion and requires the knowledge of channel state information (CSI) perfectly both at the receiver and transmitter sites. Also, under the perfect CSI assumption, it was shown in Sec. 4 that $\mathbf{G}$ is a unit diagonal matrix. However, we now show that even the CSI is not perfectly known at receiver, the optimal data detection is not affected by this imperfection. Assume that the channels $\mathbf{H}_I$ are known at the receiver with an error $\mathbf{E}$. Then the estimated channel matrix $\widehat{\mathbf{H}}_I$ can be expressed in terms error-free channel matrix $\mathbf{H}_I$ as

$$\mathbf{H}_I = \widehat{\mathbf{H}}_I + \mathbf{E}.$$

Substituting this into the expression of $\mathbf{G}$ above we have

$$\begin{aligned}\widehat{\mathbf{G}} &= (\widehat{\mathbf{H}}_I + \mathbf{E})\left((\widehat{\mathbf{H}}_I + \mathbf{E})^T(\widehat{\mathbf{H}}_I + \mathbf{E})\right)^{-1}(\widehat{\mathbf{H}}_I + \mathbf{E})^T \\ &= \mathbf{I}_{N_r} \end{aligned} \tag{6.2}$$

The second equation in (6.2) follows due to the fact that for any matrices $\mathbf{A} \in \mathcal{R}^{N\times N}$ and $\mathbf{B} \in \mathcal{R}^{N\times M}$ it is true that $\mathbf{A} = \mathbf{B}\left(\mathbf{B}^T\mathbf{B}\right)^{-1}\mathbf{B}^T = \mathbf{I}_N$. This can be shown easily by multiplying $\mathbf{A}$ with $\mathbf{B}^T$ from the left side and observing that $\mathbf{B}^T\mathbf{A} \equiv \mathbf{B}^T$ if $\mathbf{A} = \mathbf{I}_N$. Consequently, transmitted data can be recovered optimally by the maximum likelihood (ML) detection using the received signal

$$\mathbf{y}_B = \beta\mathbf{x} + \mathbf{w}_B$$

However, true value of β is not known at the receiver and hence needs to be estimated as accurate as possible from the received signal $\mathbf{y}_B$, by means of some pilot GSSK symbols prior to data detection at receiver. This is accomplished as explained the following subsection.

6.1 ML Estimations of β

From the observation equation (6.1) at receiver, for the pilot symbols $\mathbf{x} = \mathbf{s}_p$ $\left(\mathbf{s}_p \text{ that are chosen from } \{\widetilde{\mathbf{h}}_{I,\text{eff}}\} \text{ for } I = 1, 2, \cdots N_a\right)$, the conditional probability density function (pdf) $\mathbf{y}_B$, given β can be expressed as

$$p(\mathbf{y}_B|\beta) \sim \exp\left(-\frac{1}{2\sigma_w^2}|\mathbf{y}_B - \beta\mathbf{s}_p|^2\right), \quad p = 1, 2, \cdots, P. \tag{6.3}$$

Maximizing (6.1) with respect to β, the ML estimate of β can be obtained as

$$\widehat{\beta}_{ML} = \frac{\mathbf{y}_B^T\mathbf{s}_p}{||\mathbf{s}_p||^2}. \tag{6.4}$$

6.2 Computer Simulations for BER Analysis Under Imperfect CSI

In this section, BER performance of the proposed PLS algorithm is investigated in the presence of imperfect CSI. Using the estimated values for β in the PLS

algorithm, BER vs. SNR curves are obtained to examine whether the algorithm is capable of maintain its secrecy rate performance under the imperfect CSI case.
Computer simulation results are obtained for the BER performances of the legitimate users as well as the eavesdroppers, at different SNR values for different scenarios based on different locations and geometry of the luminaries, as well as the different positions of the user and the number of receivers and the eavesdropper on the floor. In the simulation setups given below, each fixture surrounds 7 LEDs located around the fixture, and 1 W optical power radiates by each LED. The half-power semi angle of each LED is 60^o.The configurations of each PD's field of view (FoV) assumed to be 70^o and physical areas of these PDs are assumed to be 1 cm^2. The reflectance coefficients of the floor and walls materials are selected as 0.3 and 0.8, respectively.
As shown in the Figure 4.2, a $5 \times 5 \times 3$ m^3 room is considered and there are 8 uniformly distributed fixtures on the ceiling of the room to illuminate this room. That is, $N_t = 8$. Locations of these fixtures are given as;

$$\mathbf{p}_{\text{tx}} = \begin{bmatrix} 1.5 & 1.5 & 1.5 & 1.5 & -1.5 & -1.5 & -1.5 & -1.5 \\ -2.25 & -0.75 & 0.75 & 2.25 & -2.25 & -0.75 & 0.75 & 2.25 \end{bmatrix}. \tag{6.5}$$

In the computer simulations, it is assumed that each receiver is equipped with 2 PDs placed at a height of 0.85 m and separated by a distance of 3 cm. These simulation studies are carried out for three different scenarios as Section 4, same as the scenarios of the previous simulations. Depending on the locations of users and their distance from each other, simulation results were obtained by these scenarios as follows.

***Scenario 1*:** In the indoor geometry shown in Figure 4.2 (a), the locations of the receivers are selected as $[-2.2], [2, -2]$ meters. The MIMO channel matrix for receiver Bob and Eve are given below.

$$\mathbf{H}_{\text{B}} = 10^{-5} \times \begin{bmatrix} 6.6036 & 4.0374 & 1.5469 & 1.0099 & 1.0919 & 1.0458 & 0.8438 & 0.72101 \\ 7.4745 & 4.4703 & 1.6317 & 1.0434 & 1.2341 & 1.1560 & 0.8926 & 0.7500 \end{bmatrix}.$$

$$\mathbf{H}_{\mathrm{E}} = 10^{-5} \times \begin{bmatrix} 0.7355 & 0.8699 & 1.1410 & 1.2275 & 1.0433 & 1.6269 & 4.4093 & 7.46671 \\ 0.7159 & 0.8307 & 1.0418 & 1.0930 & 1.0012 & 1.5440 & 4.0112 & 6.5833 \end{bmatrix}.$$

***Scenario 2*:** In the indoor geometry shown in Figure 4.2 (b), the locations of the receivers are selected as $[-2.5, -0.5], [1.5, 0]$ meters. The MIMO channel matrix for receiver Bob and Eve are given below.

$$\mathbf{H}_{\mathrm{B}} = 10^{-5} \times \begin{bmatrix} 2.3909 & 1.3824 & 0.6885 & 0.4763 & 3.4712 & 1.7520 & 0.7627 & 0.5051 \\ 1.6461 & 1.0828 & 0.6166 & 0.4454 & 4.7690 & 2.1299 & 0.8271 & 0.5291 \end{bmatrix}.$$

$$\mathbf{H}_{\mathrm{E}} = 10^{-5} \times \begin{bmatrix} 1.1441 & 1.7189 & 3.5014 & 4.0126 & 1.0660 & 1.4846 & 2.5946 & 2.8974 \\ 1.0657 & 1.4845 & 2.5963 & 2.8992 & 1.1448 & 1.7188 & 3.5021 & 4.0142 \end{bmatrix}.$$

***Scenario 3*:** In the indoor geometry shown in Figure 4.2 (c), the locations of the receivers are selected as $[-2.5, -0.5], [1.5, 0]$ meters. The MIMO channel matrix for receiver Bob and Eve are given below.

$$\mathbf{H}_{\mathrm{B}} = 10^{-5} \times \begin{bmatrix} 2.0514 & 3.3091 & 3.3086 & 2.0510 & 1.7306 & 2.4587 & 2.4610 & 1.73181 \\ 1.7305 & 2.4602 & 2.4602 & 1.7306 & 2.0529 & 3.3086 & 3.3110 & 2.0552 \end{bmatrix}.$$

$$\mathbf{H}_{\mathrm{E}} = 10^{-5} \times \begin{bmatrix} 1.4627 & 2.4004 & 3.8357 & 2.9738 & 1.3101 & 1.9238 & 2.7576 & 2.3225 \\ 1.3101 & 1.9253 & 2.7579 & 2.3202 & 1.4635 & 2.4001 & 3.8371 & 2.9795 \end{bmatrix}.$$

6.3 Computer Simulations

At different SNR values, the BER performance curves of Bob and Eve in all three scenarios are obtained and depicted in Figures 6.1 and 6.2 for the PLS

algorithm employed in the OGSSK-based VLC system. Namely, BER vs. SNR performances for the noise variance=10^{-1} and 10^{-3} are shown in Figures 6.1 and 6.2, respectively.

For the both cases - the perfect CSI and the noise in the channel are taken into con-

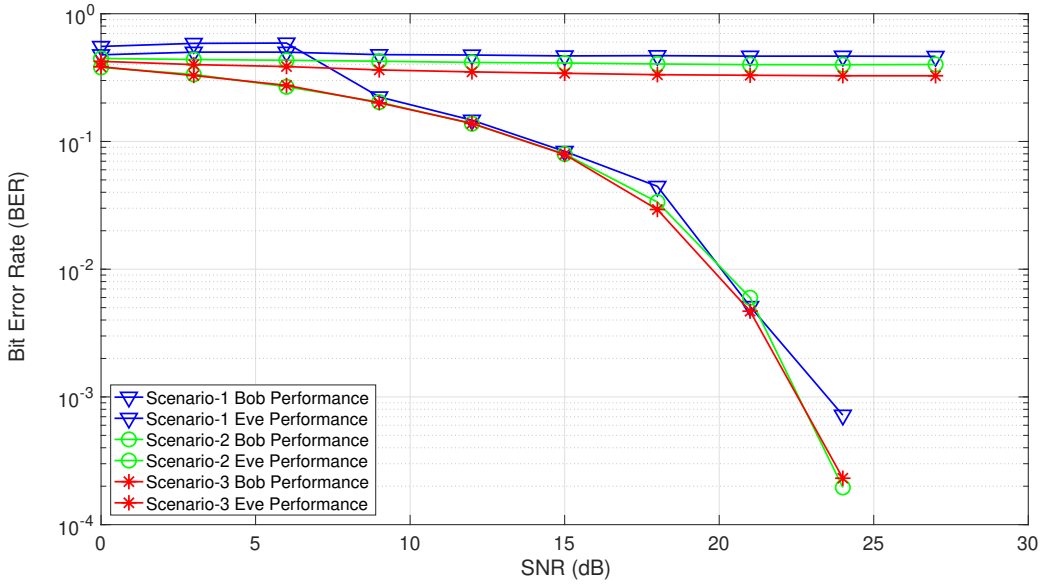

Figure 6.1 BER vs. SNR performances for Bob and Eve in an OGSSK-based VLC system with the noise with variance=10^{-1}

sideration - it is concluded that the presented PLS algorithm has an excellent BER performance and thus a secure communication can be provided easily in both cases. It is observed that the system has better BER performance in low noise variance values (eg: variance=10^{-3}) compared to the large variance values (eg: variance=10^{-1}).

A comparison of BER and SNR performance in the case of perfect and imperfect CSI corresponding to Scenario-2 is shown in Figure 6.3. Here, it is clearly shown that the algorithm performs well even in case of imperfect CSI.

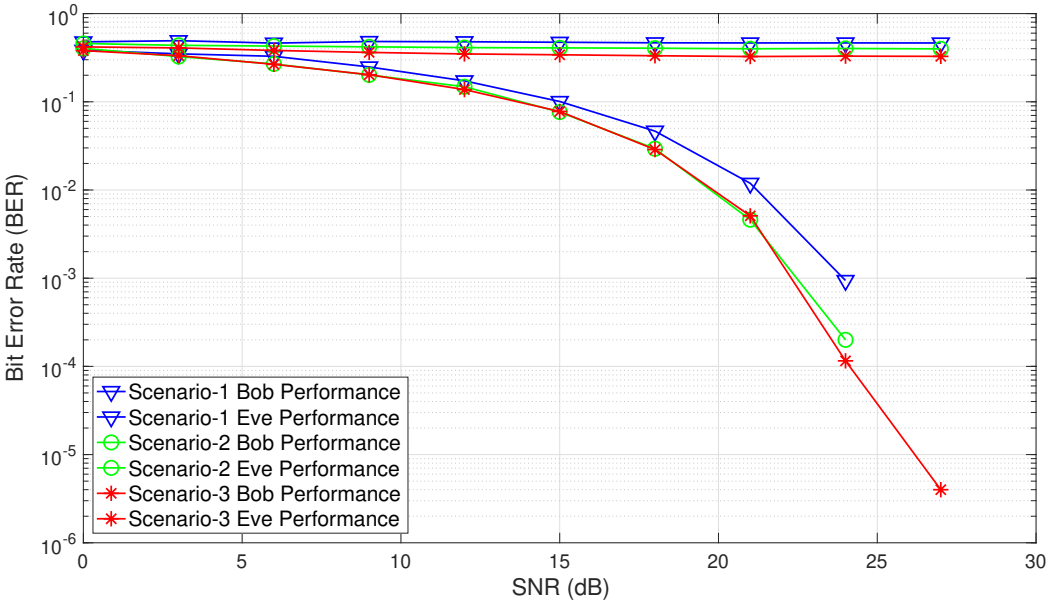

Figure 6.2 BER vs. SNR performances for Bob and Eve in an OGSSK-based VLC system with the noise with variance=10^{-3}

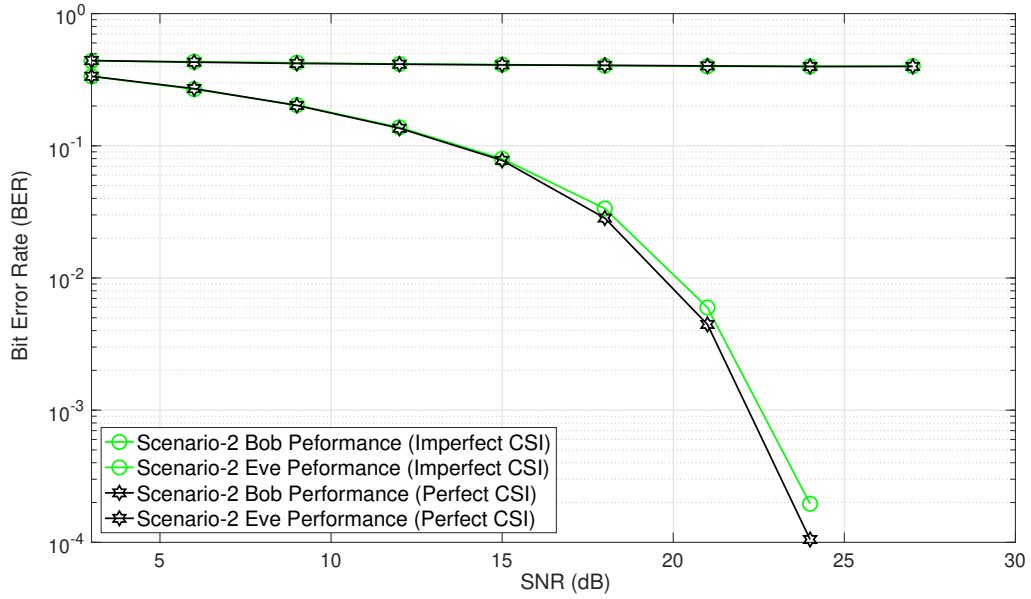

Figure 6.3 Comparison of BER vs. SNR performance in case of perfect and imperfect CSI corresponding to the Scenario-2

7. CONCLUSIONS

In this thesis, in Chapter 1, a literature review for VLC and PLS for OWC is presented and main contributions of the thesis is highlighted. In Chapter 2, working principle of VLC is introduced, including IM/DD structure, Light Emitted Diode (LED) and Photodiode (PD) which are used as essential parts of transmitter and receiver. Basic PLS techniques employed in VLCs were explained in Chapter 3 by considering different communication scenarios. In Chapter 4, the PLS algorithm, developed for OGSSK based VLC systems, was explained in detail and tested for different communication scenarios. With computer simulations, the proposed PLS algorithm has been shown to have excellent performance in the presence of perfect CSI case. In Chapter 5, a new and novel iterative channel estimation algorithm was proposed for estimation of sparsely modelled indoor VLC channels under the effect of clipping noise. Both MSE performance of this algorithm and the system BER performance in transmission performed with a VLC system using DCO-OFDM technique have been examined by computer simulations. While the initial channel estimation was implemented by means the pilot symbols, in each iteration step, the clipping noise was estimated by using the previous channel values and the effect was compensated in the frequency-domain. The results obtained in computer simulations are as follows:

- It was shown that the algorithm is very effective in minimizing the effect of inevitable clipping noise especially affecting these systems. In particular, MSE and BER performances of the system for different clipping noise levels for DCO-OFDM systems over sparse VLC channels were investigated and was found that the algorithm reached the maximum performance of the system in two iterations, at most.

- It was also concluded that the system had better BER performance for lower SNR values at low clipping noise levels, but higher SNR values showed significantly better BER performance for higher SNR values.

In Chapter 6, an effective, computationally efficient and powerful PLS algorithm has been proposed in OGSSK-based VLC systems for single legitimate user and one eavesdropper case. It was verified by the extensive computer simulations that excellent security performance could be obtained in the presence of perfect CSI case. The BER and secrecy rate performances of algorithm was examined also when the CSI was not known perfectly during data detection at receiver. It was shown that the channel normalizing constant β, unknown at the receiver end, was the only parameter that was affecting the performance of he algorithm. A pilot-aided ML parameter estimation algorithm was introduced that estimated β in an efficient way at the receiver. The computer simulation based on the estimates of the unknown channel parameters has shown excellent BER and secrecy performances to ensure physical layer security in the case of imperfect CSI. The developed algorithm has was under different SNR values as well as for different locations of the legitimate and eavesdropper during data transmission. It was with the computer simulations that the algorithm performs very well even in case of imperfect CSI for different scenarios.
The other results obtained by computer simulation are as follows:

- The perfect and imperfect CSI cases were examined together and it was clearly shown that the developed algorithm performed in the presence of imperfect CSI was very close to the perfect CSI performance for the perfect CSI case.
- In the simulation results for different variance values of the channel noise, it was concluded that the system had better BER performance at low SNR values.

7.1 Future Work

In this thesis a new channel estimation algorithm for DCO-OFDM based VLC system is investigated in wide sense (presented in Chapter 5). This work could be extended for the OGSSK based VLC systems.

In Chapter 4 and 6, a new PLS technique for OGSSK based VLC system is presented. New PLS techniques could be developed for different VLC systems (eg.; NOMA VLC systems) in the future works. Also, uncertain in CSI could be analysed for new PLS techniques.

REFERENCES

1. A.G. Bell, "Selenium and the Photophone," *Nature*, vol. 22, pp. 500–503, 1880.
2. N. Sklavos, M. Hubner, D. Goehringer and P. Kitsos, *System-Level Design Methodologies for Telecommunication*, Springer, Berlin, Germany, 2014.
3. A.R. Ndjiongue, T. Ngatched and H.C. Ferreira, *Visible Light Communications (VLC) Technology*, Hoboken, NJ, USA: Wiley, 2000.
4. A. Mostafa and L. Lampe, "Physical-layer security for indoor visible light communications," *IEEE International Conference on Communications (ICC)*, Sydney, NSW, 2014, pp. 3342-3347, 2014.
5. M.A. Arfaoui, M.D. Soltani, I. Tavakkolnia, A. Ghrayeb, C. Assi, M. Safari and H. Haas, "Physical Layer Security for Visible Light Communication Systems: A Survey," in *IEEE Communications Surveys and Tutorials*, doi: 10.1109/COMST.2020.2988615.
6. C. E. Shannon, “Communication theory of secrecy systems,” *Bell Syst. Tech. J.*, vol. 28, no. 4, pp. 656–715, Oct. 1949.
7. A. D. Wyner, "The wire-tap channel," *Bell Syst. Tech. J.*, vol. 54, no. 8, pp. 1355-1387, Oct.1975.
8. S. Leung-Yan-Cheong and M. Hellman, "The Gaussian wire-tap channel," in *IEEE Transactions on Information Theory*, vol. 24, no. 4, pp. 451-456, July 1978.
9. E. B. Bektas, E.Panayirci, "Sparse Channel Estimation with Clipping Noise in DCO-OFDM Based VLC Systems," *IEEE International Black Sea Conference on Communications and Networking (BlackSeaCom)*, Odessa, Ukraine (Virtual), 2020.
10. J. M. Kahn and J. R. Barry, "Wireless infrared communications," in *Proceedings of the IEEE*, vol. 85, no. 2, pp. 265-298, Feb. 1997.
11. Ghassemlooy, Z.; Popoola, W.; Rajbhandari, *S. Optical Wireless Communications: System and Channel Modelling with MATLAB*; CRC Press: Boca Raton, FL, USA, 2013.
12. Knutson, C. D.; Brown, J. M. *IrDA Principles and Protocols*, MCL Press, 0-

9753892-0-3, USA, 2004.

13. Jeffrey B. Carruthers, “Wireless Infrared Communications,” *Wiley Encyclopedia of Telecommunications*, 2002.
14. I. Csiszar and J. Korner, "Broadcast channels with confidential messages," in *IEEE Transactions on Information Theory*, vol. 24, no. 3, pp. 339-348, May 1978.
15. J. G. Smith, “The information capacity of amplitude and variance-constrained scalar Gaussian channels,” *Journal of Information and Control*, vol. 18, pp. 203–219, 1971.
16. S. Hranilovic and F. Kschischang, “Optical intensity-modulated direct detection channels: Signal space and lattice codes,” *IEEE Transactions on Information Theory*, vol. 49, no. 6, pp. 1385–1399, Jun. 2003.
17. A. Lapidoth, S. Moser, and M. Wigger, “On the capacity of free-space optical intensity channels,” *IEEE Transactions on Information Theory*, vol. 55, no. 10, pp. 4449–4461, Oct. 2009.
18. S. Dimitrov and H. Haas, "Information Rate of OFDM-Based Optical Wireless Communication Systems With Nonlinear Distortion," in *Journal of Lightwave Technology*, vol. 31, no. 6, pp. 918-929, March15, 2013.
19. C. E. Shannon, “A mathematical theory of communication,” *Bell Syst. Tech. J.*, vol. 27, no. 3, pp. 379–423, Jul./Oct. 1948.
20. A. Mostafa and L. Lampe, "Physical-layer security for indoor visible light communications," *IEEE International Conference on Communications (ICC)*, Sydney, NSW, 2014, pp. 3342-3347, 2014.
21. O. Ozel, E. Ekrem and S. Ulukus, "Gaussian Wiretap Channel With Amplitude and Variance Constraints," in *IEEE Transactions on Information Theory*, vol. 61, no. 10, pp. 5553-5563, Oct. 2015.
22. A. Mostafa and L. Lampe, "Physical-Layer Security for MISO Visible Light Communication Channels," in *IEEE Journal on Selected Areas in Communications*, vol. 33, no. 9, pp. 1806-1818, Sept. 2015.
23. H. Zaid, Z. Rezki, A. Chaaban and M. S. Alouini, "Improved achievable secrecy rate of visible light communication with cooperative jamming," *IEEE Global*

Conference on Signal and Information Processing (GlobalSIP), Orlando, FL, 2015, pp. 1165-1169, 2015.

24. M. A. Arfaoui, Z. Rezki, A. Ghrayeb and M. S. Alouini, "On the Secrecy Capacity of MISO Visible Light Communication Channels," *IEEE Global Communications Conference (GLOBECOM)*, Washington, DC, 2016, pp. 1-7, 2016.
25. A. Yesilkaya, T. Cogalan, S.Erkucuk, Y. Sadi, E. Panayirci, H. Haas and H. V. Poor, "Physical-Layer Security in Visible Light Communications," *2nd 6G Wireless Summit*, 2020.
26. A. Mostafa and L. Lampe, "Securing visible light communications via friendly jamming," *2014 IEEE Globecom Workshops (GC Wkshps)*, Austin, TX, 2014, pp. 524-529, doi: 10.1109/GLOCOMW.2014.7063485.
27. F. Wang, R. Li, J. Zhang, S. Shi, and C. Liu, "Enhancing the secrecy performance of the spatial modulation aided VLC systems with optical jamming," *Signal Process.*, vol. 157, pp. 288 – 302, Dec. 2019.
28. L. Wang, S. Bashar, Y. Wei, and R. Li, "Secrecy enhancement analysis against unknown eavesdropping in spatial modulation," *IEEE Commun. Lett.*, vol. 19, no. 8, pp. 1351–1354, Aug 2015.
29. E. Başar, Ü. Aygölü, E. Panayırcı and H. V. Poor, "Orthogonal frequency division multiplexing with index modulation," *2012 IEEE Global Communications Conference (GLOBECOM)*, Anaheim, CA, 2012, pp. 4741-4746, doi: 10.1109/GLOCOM.2012.6503868.
30. R. Mesleh, H. Elgala and H. Haas, "Optical Spatial Modulation," in *IEEE/OSA Journal of Optical Communications and Networking*, vol. 3, no. 3, pp. 234-244, March 2011, doi: 10.1364/JOCN.3.000234.
31. W. O. Popoola, "Merits and limitations of spatial modulation for optical wireless communications," *2013 2nd International Workshop on Optical Wireless Communications (IWOW)*, Newcastle upon Tyne, 2013, pp. 152-156, doi: 10.1109/IWOW.2013.6777797.
32. W. Popoola, E. Poves and H. Haas, "Generalised space shift keying for visible light communications," *2012 8th International Symposium on Communication Systems, Networks & Digital Signal Processing (CSNDSP)*, Poznan, 2012, pp.

1-4, doi: 10.1109/CSNDSP.2012.6292784.

33. S. Dissanayake and J. Armstrong, “Comparison of ACO-OFDM, DCO-OFDM and ADO-OFDM in IM/DD systems," *Journal of Lightwave Technology*, vol. 31, no. 7, pp. 1063–1072, Apr. 2013.
34. J. J. Bussgang. “Crosscorrelation functions of amplitude-distorted Gaussian signals," *Tech. Rep. 216*, Department of Computer Science, Michigan State University, March 1952.
35. S. C. Schwartz, J. Zhang and D. Gu, "Iterative channel estimation for OFDM with clipping," *The 5th Int. Symp. Wireless Personal Multimedia Communications*, pp. 1304-1308 vol.3, Honolulu, HI, USA, 2002.
36. J. Armstrong and B. J. C. Schmidt, “Comparison of asymmetrically clipped optical ofdm and dc-biased optical ofdm in awgn,” *IEEE Communications Letters*, vol. 12, no. 5, pp. 343–345, May 2008.

CURRICULUM VITAE

Ekin Basak Bektas was born on 4 January 1996, in Istanbul. She received her B.Sc. degree in Electrical & Electronics Engineering in 2018 from Kadir Has University. Then, she continued her M.Sc. degree in Electronics Engineering at Kadir Has University, where she worked as a teaching assistant at the Department of Electrical-Electronics Engineering from 2018 to 2020. Her research interests include signal processing and wireless communication.

Publications:

- *E. B. Bektas, E.Panayirci, "Channel Estimation for DCO-OFDM Based VLC Systems in the Presence of Clipping Noise," *28th Signal Processing and Communications Applications Conference (SIU)*, Gaziantep, Turkey, **(Accepted)**, 2020 (in Turkish).
- *E. B. Bektas, E.Panayirci, "Sparse Channel Estimation with Clipping Noise in DCO-OFDM Based VLC Systems," *IEEE International Black Sea Conference on Communications and Networking (BlackSeaCom)*, Odessa, Ukraine (Virtual), 2020.